UNIVERSITY OF CALIFORNIA SAN DIEGO

# Design and delivery of nanoscale therapeutics for myocardial infarction

A Dissertation submitted in partial satisfaction of the
requirements for the degree Doctor of Philosophy

in

Bioengineering

by

Holly Sullivan

Committee in charge:

Professor Karen L. Christman, Chair
Professor Barry Greenberg
Professor Ester Kwon
Professor Prasant Mali
Professor Nicole Steinmetz

2022

The Dissertation of Holly Sullivan is approved, and it is acceptable in quality and form for publication on microfilm and electronically.

University of California San Diego

2022

## DEDICATION

To my mom.

**TABLE OF CONTENTS**

## LIST OF ABBREVIATIONS

ACT: Activated clotting time

$\alpha$-SMA: Alpha smooth muscle actin

ANOVA: Analysis of Variance Test

CHP: Cardiac homing peptide

CM: cell membrane

DLS: dynamic light scattering

DPBS: Dulbecco's phosphate buffered saline

DMSO: dimethyl sulfoxide

H&E: Hematoxylin and eosin

IV: intravenous

IP: intraperitoneal

MePTDO: 1,3-dimethyl-2-phenoxy-1,3,4,7-tetrahydro-1,3,2-diazaphosphepine 2-oxide

MI: Myocardial infarction

MMP: matrix metalloproteinase

MMPi: MMP inhibitor

NorMMPi: Norbornene matrix metalloproteinase inhibitor

NP: Nanoparticle

PI: propidium iodide

PLP: Protein-like polymer

PPA: peptide polymer amphiphile

ROMP: Ring-opening metathesis polymerization

TEM: transmission electron microscopy

XO: Exosome

ZDEC: zinc diethyldithiocarbamate

## LIST OF FIGURES

## LIST OF TABLES

## ACKNOWLEDGEMENTS

This whole process has involved the help and encouragement of many throughout the many stages of graduate school.

First, I would like to thank my adviser, Karen Christman, for taking me on as a student all those years ago. I remember how badly I wanted to be a part of her lab—so much so that I wrote my NSF GRFP proposal with her work in mind before I even got into UCSD's bioengineering program. I have appreciated the opportunity being in her group has given me. Additionally I would like to thank my thesis committee, Ester Kwon, Nicole Steinmetz, Prashant Mali, and Barry Greenberg, for their feedback and support through this process.

Perhaps just as impactful than the opportunity for research were the people that I got to work with. All of my lab mates have been instrumental in the build-up of my PhD. Dr. Pamela Duran, Dr. Martin Spang, Miranda Diaz, Jervaughn Hunter, Emma Zelus, and Joshua Mesfin were all around for the bulk of my time at UCSD and were invaluable when I needed another person to vent to or troubleshoot with. Dr. Gina Policastro and Dr. Jessica Ungerleider were among the first people in the lab that I was able to work with, and I appreciate their openness and patience as they introduced me to the lab and made me feel comfortable and welcome.

Throughout my work, I collaborated strongly with the Gianneschi lab at Northwestern University and would be remiss if I did not acknowledge their influence on my work. Nathan Gianneschi, Yifei Liang, Spencer Burton, Matthew Thompson, and Andrea Carlini have all taught me so much about the field of polymer chemistry and infused great interdisciplinary knowledge into my experiments. Truly none of this work could have been accomplished without their contribution.

Though most of the science happens inside the lab, a lot of my person growth during this time happened outside of the lab. My friends and lab mates who play double-duty as friends: Dana Nachmanson, Jeffry Granados, Rachel Lindley, Deval Gupta, Clara Posner, Michael Wiest, Lindsey Bergh, Sara Mirza, Kristi Chan, Emma Imhof, Miranda Diaz, and Pamela Duran have been instrumental in helping me logic through not only my research problems but also my life in general. They have helped me through the lows and celebrated with me during the highs, and that has meant a lot to me. I have so appreciated the time spent talking, texting, working out, traveling, reading books, or drinking coffee together over the years and I know I would be a different person without them in my life. I also want to thank my friend-turned-partner, Michael Sveiven, who is my favorite person to talk to about pretty much anything.

Of course, this could not have been done without the support of my mom—who has shown endless support in literally anything I've ever expressed interest in (figure skating, acting, gymnastics, piano, etc). I have always felt that any possibility was within reach because of her, and I think that has given me the persistence I needed to finish something as mammoth as this.

On a lighthearted note, I'd like to thank all the various coffee shops that housed me as I put together 5 years of research into this one document. I'd also like to acknowledge my little cat, Tofu, who is sitting on my lap now and has kept me company for the last 4 years while helping me remember that even if there are days that I feel I'm not an excellent scientist, I am still a pretty good cat-mom. Additionally, I'd like to thank my therapist, Katarina Mansir, for listening to me as I stomped through my neighborhood on therapy walks for the last two and a half years and helping me become a more thoughtful and braver version of myself.

Chapter 1 is part of a paper that has been published as a review paper in Biomaterials Science, Holly Sullivan, Nathan C. Gianneschi, Karen L. Christman. “Targeted nanoscale therapeutics for myocardial infarction”. The dissertation author was the first author of this papers.

Chapter 2 is currently being prepared for submission for publication of the material, Holly Sullivan, Yifei Liang, Kendra Worthington, Colin Luo, Nathan C. Gianneschi, Karen L. Christman. “Enzyme-Responsive Nanoparticles for the Targeted Delivery of an MMP Inhibitor to the Heart post Myocardial Infarction”. The dissertation author is the co-first author of this paper.

Chapter 3 is currently being prepared for submission for publication of the material, Holly Sullivan, Yifei Liang, Kendra Worthington, Colin Luo, Nathan C. Gianneschi, Karen L. Christman. “Degradable Poly(phosphoramidate): Efficient Synthesis, Peptide Functionalization, and Targeted Delivery to the Infarcted Heart”. The dissertation author will be a co-first author of this paper.

Chapter 4 is currently being prepared for submission for publication of the material, Holly Sullivan, Spencer Burton, Kendra Worthington, Colin Luo, Nathan C. Gianneschi, Karen L. Christman. “Protein-like polymers for targeted delivery to the infarct after acute myocardial infarction”. The dissertation author will be a co-first author of this paper.

## VITA

2017 Bachelor of Science in Chemical Engineering at the University of Washington, Seattle, WA

2022 Doctor of Philosophy in Bioengineering at University of California San Diego

PUBLICATIONS

**Sullivan HL***, Liang Y*, Worthington K, Luo C, Gianneschi NC, Christman KL. Enzyme-Responsive Nanoparticles for the Targeted Delivery of an MMP Inhibitor to the Heart post Myocardial Infarction. *bioRxiv*, 2022.2003.2007.483374, doi:10.1101/2022.03.07.483374 (2022).

**Sullivan HL**, Gianneschi NC, Christman KL. Targeted nanoscale therapeutics for myocardial infarction. *Biomaterials Science* **9**, 1204-1216, doi:10.1039/D0BM01677B (2021).

## ABSTRACT OF THE DISSERTATION

Design and delivery of nanoscale therapeutics for myocardial infarction

by

Holly Sullivan

Doctor of Philosophy in Bioengineering

University of California San Diego, 2022

Professor Karen L. Christman, Chair

Myocardial infarction (MI) affects nearly 800,000 people every year in the United States. As it stands, treating patients during the acute phase of MI is highly limited due to the fragility of the infarcted heart. Thus, minimally invasive intravenous administration of targeted nanoscale therapeutics has the potential to allow for more effective treatment of the heart during this acute phase of MI, a therapeutic window in which more invasive procedures are not feasible. Using an

ischemia-reperfusion injury model in rats, we assessed three different nanoscale platforms: polynorbornene nanoparticles, a degradable copolymer nanoparticle, and a polynorbornene protein-like polymer. All these systems leverage the enhanced permeability and retention effect in the infarcted region of the heart and extravasates into the injured myocardium, undergoing a morphological switch from the nano to the micron-scale when cleaved by endogenous MMPs in the infarct. First, we demonstrated the aggregation and localization of matrix metalloproteinase (MMP) responsive peptide-polymer amphiphile polynorbornene nanoparticles carrying a small molecule MMP-inhibitor to the heart following acute myocardial infarction (MI). In addition, we showed that drug incorporation onto the nanoparticle backbone improved significantly improved it's the maximum concentration at which it could be tolerated compared to free drug treatment *in* vitro while also maintain the drug's bioactivity. Next, we assess the degradable nanoparticle for cytocompatibility, infarct-localization, and biodistribution over time. We found that this material successfully degrades over time while exhibiting distinct and beneficial biodistribution compared to previous work. Lastly, we investigated the biodistribution and mechanism of accumulation using a protein-like polymer. We observed strong colocalization of this material with necrotic cardiomyocytes in the infarcted region and favorable biodistribution that preferentially biased accumulation in the kidneys over other satellite organs. All these material approaches are highly versatile and can be easily adapted to carry various therapeutic payloads, making them a potential platform for targeted drug delivery to areas of inflammation.

# Chapter 1: Targeted nanoscale therapeutics for myocardial infarction

## 1.1 Introduction

Nanoscale therapeutics have promise for the administration of therapeutic small molecules and biologics to the heart following myocardial infarction. Directed delivery to the infarcted region of the heart using minimally invasive routes is critical to this promise. In this review, we will discuss the advances and design considerations for nanoparticle therapeutics engineered to target the infarcted heart.

In 2017, ischemic heart disease affected almost 126 million people globally and led to the death of nearly 9 million people, making it the leading cause of mortality in the world[1]. While ischemic heart disease represents various clinical conditions, one of its primary manifestations is myocardial infarction (MI). Though techniques have been developed that aid in revascularization and mitigation of further tissue damage after an MI, these practices do not promote cardiac repair. Biomaterial platforms and gene therapy have emerged as exciting regenerative medicine methods for treating the heart post-MI. The administration of therapeutics to the heart can be achieved in various ways. Intramyocardial injection can be performed by surgically opening the chest but can also be done via a transendocardial injection catheter. This method is not a good option for administration to the heart during the acute phase of MI as the heart is more prone to arrhythmias and the wall is at higher risk of rupture[2-6]. Another option is intracoronary infusion, which is performed via catheterization. While these catheter-based techniques are less invasive, intracoronary infusion allows for less control of material dissemination and transendocardial injections are technically challenging[7].

The current clinical standard of care for patients during the acute phase of MI includes angioplasty, stenting, and administration of pharmaceuticals[8]. While these methods are useful in initiating reperfusion and reducing oxygen demand in the heart, they are not able to address imbalances within the heart that arise due to ischemic damage. There is a need for therapies

that can be safely administered to patients while also delivering novel therapeutic payloads that are capable of addressing physiological issues that are present on the cellular level. Current bioengineering-based strategies in the form of cardiac patches or injectable biomaterials[9, 10] have shown therapeutic efficacy but are more suited towards patients in the sub-acute and chronic phases of MI as they require surgical or transendocardial delivery.

Ideally, administration of therapeutics post-MI should be less invasive or non-invasive, as accomplished through methods like intravenous (IV) injection or oral ingestion. However, systemic administration of therapeutics often faces limitations in efficacy due to off-target effects and short circulation times. To further complicate these issues, many of the therapeutics are not water-soluble, limiting their physiological application *in vivo*[11, 12]. These issues go beyond small molecules. Cardiovascular medicine has become increasingly focused on the use of biologics (miRNAs, therapeutic transgenes, siRNAs, etc)[13-15]. These payloads face their own and parallel issues with the aforementioned small molecule drugs—limited efficacy with off-target effects and short circulation times. To overcome these challenges, drugs and biologics can be packaged into various delivery platforms that have been modified to accumulate at the site of interest, decreasing the necessary dose and mitigating off-target effects.

Properly designed nanoparticles have been shown to improve the delivery of various therapeutic payloads to the heart after MI. During the ischemic period, there is a decrease in flow-related shear stress on luminal endothelial cells—resulting in abnormal endothelial-dependent relaxation and enhanced permeability[16-19]. Nanoparticle delivery to the heart relies on this permeability effect for extravasation into infarcted tissue, but retention must be improved through the use of a specific targeting mechanism. In this review, we will discuss the current state of the field and utility of nanoparticles as nanoscale therapeutics that can be administered minimally invasively to treat MI (**Figure 1.1**). Specifically, we will focus on the

design elements that are taken into consideration when developing these nanoscale therapies.

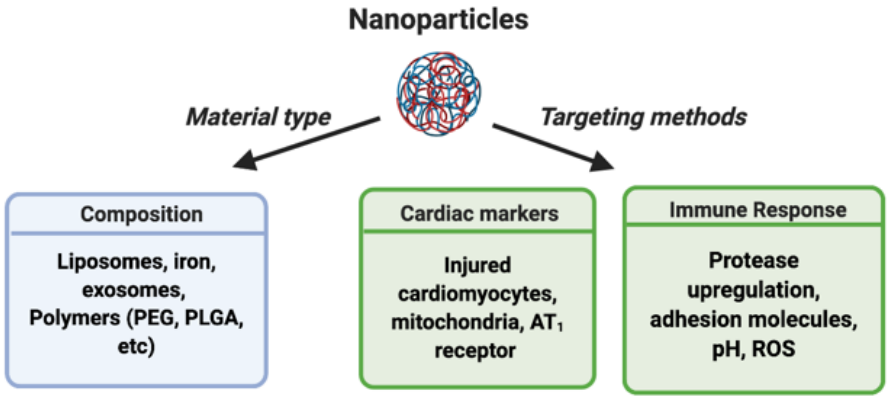


**Figure 1. 1: Nanoscale therapeutics used for cardiac applications.**
Nanoparticles of various compositions and serotypes can be modified for improved delivery to the heart post-MI.

### 1.2 Nanoparticles that target the infarcted region of the heart

Nanoparticle therapeutics have emerged as a novel way to revitalize therapeutics that have limited *in vivo* application due to poor solubility or deleterious side effects. Incorporating therapeutic payloads into a nanoparticle system has been shown to increase circulation time and improve therapeutic retention in preclinical models[20, 21]. While the preclinical research and clinical trial landscape for nanoparticle therapeutics has been overwhelmingly ruled by cancer applications[22], the field is becoming more diverse. Nanomedicine for cardiovascular applications is newer than in oncology but is seeing rapid development and growth[23]. Since 2016, two nanoparticle platforms have been approved by the FDA for imaging applications post-MI[24] but there have not been any FDA approved nanoparticle platforms for treatment of the infarcted heart. Nanomedicine was initially seen as a way to increase drug circulation time and reduce systemic toxicity. However, as the field has advanced, materials have become increasingly complex with more functionalization to aid in site-specific delivery. Though this

increased in design complexity has led to a slowdown in clinical progress[23], it will allow for the development of more effective nanoparticle platforms that can traffic through the body safely and accumulate in the infarcted region for optimal efficacy. Here we will discuss nanoparticle targeting methods into two main categories, designs that take advantage of the immune response and those that are created to interact with cardiac-specific features (**Table 1.1**).

While nanoparticles have increased circulation time compared to freely administered small molecules and biologics, they are still subject to off target accumulation, specifically in satellite organs such as the kidneys and liver; organs designed to clear such materials, making this task inherently difficult[25]. Generally, their potential systemic effects remain a limiting factor in the clinical translation of nanoparticles. However, with thoughtful material design, it is possible to improve site-specific delivery as is seen in several cases we will highlight.

To design vehicles that target the heart, it is crucial to understand the underlying biology during and following MI (**Figure 1.2**). The upregulation of certain enzymes and cytokines as well as the influx of immune cells into the infarcted region of the heart represent unique biological signatures that can be leveraged and utilized as markers for targeting. In addition, production of reactive oxygen species (ROS) has been shown to have a significant role in the pathogenesis of vascular damage[16] and leukocyte chemotaxis[26] to the area of injury. Neutrophils are the first inflammatory cell to infiltrate into the infarct with macrophages of various subsets following at a later stage[27]. Matrix metalloproteinase (MMP) production is upregulated in the heart within 10 minutes after occlusion[27]. Out of the many types of MMPs, MMP-2 and MMP-9 are specifically upregulated during the acute phase of MI and remain at high levels of expression for months[28]. Accompanying this intense inflammatory response, there is a decrease in the pH of the heart following MI by at least a unit, from 7.4 to ~6.4[27]. These alterations in the heart microenvironment can serve as inspiration for targeted design of therapeutics.

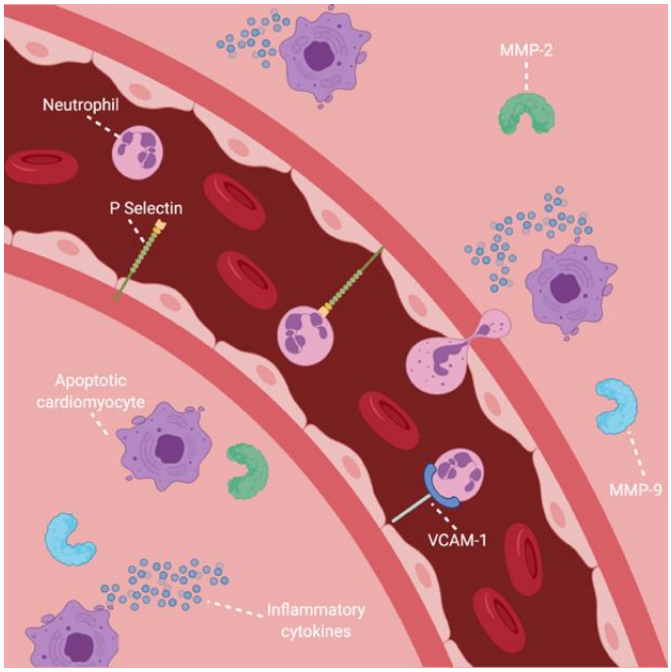


**Figure 1. 2: The inflammatory response during the acute phase of MI. The inflammatory response during the acute phase of MI.**
Hallmarks of this response include recruitment of neutrophils to the infarct via adhesion molecules P selectin and vascular cell adhesion protein 1 (VCAM-1). Additionally, matrix metalloproteinases (MMP) 2 and 9 are upregulated and begin to degrade the collagen in the heart. Apoptotic cardiomyocytes release inflammatory cytokines such as IL-6 that activate inflammatory cascades in fibroblasts, immune cells, and vascular cells.

## Table 1.1: Targeted nanoparticle therapies for MI[a]

| Authors | Material | Particle Size | Animal Model | Target | Dosage Timeline | Payload | Outcomes | Ref. |
|---|---|---|---|---|---|---|---|---|
| Scott et al. (2009) | Liposome conjugated with anti-P-selectin antibodies | 180 ± 35 nm | Myocardial infarction (permanent occlusion, rat) | P-selectin | Immediately after injury | VEGF | Targeted VEGF resulted in improved LV function and increased number of anatomical and perfused vessels. | 29 |
| Nguyen et al. (2015) | Polynorbornene backbone, peptide sequence conjugated | 15-20 nm | Myocardial infarction (ischemia-reperfusion, rat) | MMPs | 1-day post injury | N/A | Study was done as proof of concept showing nanoparticle localization in the infarcted region of the heart | 30 |
| Dong et al. (2017) | RGD modified, PEGylated solid lipid nanoparticles | 110.5 nm | Myocardial infarction (permanent occlusion, rat) | $a_v b_3$ integrin | Immediately post-injury | Puerarin | RGD-modified nanoparticles demonstrate selective accumulation in the heart compared to controls, longer circulation half-life, and significant reduction in infarct area, | 32 |
| Yao et al. (2020) | Mesoporous silica nanoparticles coated with mesenchymal stem cell membranes | ~110 nm | Myocardial infarction (ischemia-reperfusion, mouse) | ICAM-1 | Every day for 3 days post-injury | miR-21 | Membrane-coated NPs resulted in increased left ventricular ejection fraction and fractional shortening as well as reduced scar size and cellular apoptosis compared to a non-membrane coated control. | 40 |
| Cheng et al. (2014) | Iron core nanoparticles conjugated to anti-CD34 and anti-MLC antibodies | 95.7 ± 14.5nm | Myocardial infarction (ischemia- reperfusion, rat) | Endogenous bone marrow derived stem cells ($CD34^+$) and injured cardiomyocytes ($MLC^+$) | 10 minutes post-injury | N/A | Antibody targeted nanoparticles resulted in an increase in the amount of viable tissue and improved left ventricular ejection fraction. These trends were further improved with the application of a magnetic field to enhance nanoparticle targeting. | 43 |
| Vandergriff et al. (2018) | Cardiac stem cell-derived exosomes conjugated to cardiac homing peptide | ~95 nm | Myocardial infarction (ischemia-reperfusion, rat) | Hypothesized to be alpha-B crystalline | 1-day post injury | Cardiac stem cell-derived exosomes | Targeted exosomes increased ejection fraction, viable tissue, and cardiomyocyte proliferation while also decreasing infarct size. | 46 |
| Zhang et al. (2018) | Lipid-polymeric nanoparticles modified with TPP and TPGS | 140 nm | Myocardial infarction (permanent occlusion, rat) | Mitochondria | Every other day for 2 weeks post-injury | Tanoshine II-A | TPP/TPGS targeted nanoparticles showed higher drug accumulation in the heart and reduced infarct size | 48 |
| Zhang et al. (2019) | PLGA-PEG-SS31 | 54 nm | Myocardial infarction (ischemia-reperfusion, rat) | Mitochondria | 5 minutes before reperfusion | Cyclosporin A | Significantly increased localization in the heart compared to a non-targeted control, decreased cardiomyocyte apoptosis and infarction area. | 50 |
| Xue et al. (2018) | PEGylated dendrigraft poly-$_L$-lysine dendrimers modified with an $AT_1$ targeting peptide | ~50 nm | Myocardial infarction (permanent occlusion, mouse) | $AT_1$ receptor | 1-day post injury | Anti-microRNA-1 | $AT_1$ modified dendrimers significantly reduced miR-1 expression, cellular apoptosis, and infarct size. | 52 |

Targeted to immune response  Targeted to cardiac features

[a]VEGF: vascular endothelial growth factor, PEG: polyethylene glycol, TPP: triphenylphosphonium, TPGS: D-α-tocopheryl polyethylene glycol 1000 succinate, $AT_1$: angiotensin II type 1

*1.2.1 Nanoparticles that target hallmarks of inflammation and wound healing*

To determine features of the inflammatory response, we will specifically focus on physiological abnormalities in heart that are a response to hypoxia, such as increased protease activity, acidity, and vasculature damage. The most common way of imparting a targeting mechanism to a nanoparticle is via surface functionalization. Scott et al. utilized this design method by decorating the surface of immunoliposomes ($180 \pm 35$ nm) with antibodies that bind P-selectin. P-selectin, a cell adhesion molecule, exhibits increased expression in the vasculature of the infarcted region and has been used to localize the delivery of VEGF post-MI[29]. Using a rat model of MI, animals were injected with their treatment via the tail vein immediately after induction of the ischemic injury. This targeted method resulted in a significant increase in fractional shortening and improved systolic function compared to systemic free VEGF treatment, demonstrating the efficacious advantages of utilizing targeted therapies. In addition to functional improvement, a significant increase in number of vessels and number of perfused vessels in the heart compared to an untreated control was noted after 4 weeks. However, the vessels in the free VEGF group were not quantified.

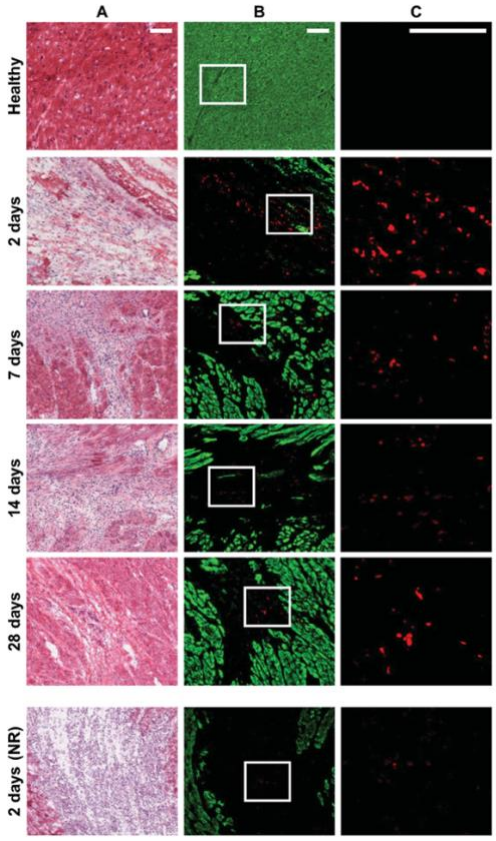


**Figure 1. 3: Enzyme responsive nanoparticles accumulate in the infarcted region of the heart.**

(A) H&E images of hearts at various time points. (B) $\alpha$-actinin (green) stained hearts following IV nanoparticle injection shows accumulation and retention of rhodamine-labelled particles (red) in infarcted areas (white boxed region) up to 28 days post-injection compared to a non-responsive (NR) nanoparticle control (bottom row). (C) Magnified boxed region from column B. Reproduced from ref. 31 with permission from WILEY - V C H VERLAGGMBH & CO. KGAA., copyright 2015.

Another robust example of surface functionalization is through the incorporation of an enzyme-responsive peptide sequence to the polymer backbone of the nanoparticle. Nguyen et al. designed peptide-polymer amphiphiles composed of a hydrophobic polymer backbone (polynorbornene) followed by the conjugation of a hydrophilic peptide sequence (GPLGLAGGWGERDGS) that is recognized and cleaved by MMP-2 and MMP-9[30]. Once cleaved, the hydrophobic core of the nanoparticle is exposed, causing aggregation from the nano-scale (15-20 nm) to the micron-scale. This morphological switch enhances nanoparticle

retention in the infarct. Nanoparticles administered via IV injection one day post-MI in a rat model showed selective aggregation of particles in the heart only when the MMP-cleavable peptide is conjugated to the polymer backbone (**Figure 1.3**). This was validated through the use of a non-responsive control peptide sequence that did not lead to nanoparticle aggregation after exposure to MMPs. While methods such as these for targeting areas of inflammation do lead to MI targeting, they are still subject to off-target accumulation due to the fact that they are not cardiac-specific and there can be other areas of active inflammation in the body.

Targeting the $\alpha_v\beta_3$ integrin, which is upregulated in endothelial cells during angiogenesis[31], is another technique that has been used to target the heart. The cyclic peptide sequence arginyl-glycyl-aspartic acid (RGD) was used to improve cell anchoring, specifically in cardiac applications. Dong et al. designed solid lipid nanoparticles (SLN)[32] covered in a layer of polyethylene glycol (PEG), a surface modification known to improve the circulation time[33], and modified the surface of the particle with the RGD peptide sequence to enable improved cell-surface binding (110.5 nm). The small molecule puerarin (PUE), a reactive oxygen species scavenger[34, 35], was encapsulated within the core of the nanoparticle. Following induction of MI via ligation of the left descending coronary artery in rats, the therapeutic efficacy and biodistribution of the RGD/PEG-PUE-SLN was compared to IV administration of saline, free drug, drug encapsulated in plain SLN, and drug encapsulated in PEGylated SLN administered immediately after injury. The RGD/PEG-PUE-SLN treated animals demonstrated increased nanoparticle accumulation in the heart compared to satellite organs and significantly decreased infarct size compared to all other treatment groups. More recently, RGD has also been used to successfully deliver miR-133 to the heart using polyethylene glycol-polylactic acid nanoparticles. It was shown to increase miR-133 levels in the infarcted area and improve heart function[36], demonstrating the versatility and function of RGD in targeting the heart acutely post-MI. However, RGD can also be used to target other

regions in the body where there is active wound healing or angiogenesis and is therefore not only cardiac-specific[37-39].

Stem cell membranes have been used as another method for targeting the infarcted heart[40]. Yao et al. designed mesoporous silica nanoparticles camouflaged with mesenchymal stem cell membranes to deliver microRNA-21, which is involved in cardiogenesis and cardiac regeneration (~110 nm). These stem cell membranes cloak the nanocomplexes from immune clearance while also imparting exosome-like qualities to this platform. Specific integrins on the membranes of mesenchymal stem cells can bind to the overexpressed intercellular adhesion molecule-1 (ICAM-1) on endothelial cells[41] and injured cardiomyocytes[42]. One day post-MI in a mouse model, these nanocomplexes were injected via the tail vein every day for three days. Whole organ imaging post-administration demonstrated strong accumulation of membrane-coated NPs in the heart (**Figure 1.4**). Functionally, administration of membrane-modified nanoparticles delivering microRNA-21 resulted in a significant increase in ejection fraction and fractional shortening as well as a reduction in myocardial scar size and cellular apoptosis compared to a non-targeted control. There was also a significant increase in Ki67 positive cardiomyocytes in the injured region of MI hearts in response to membrane-cloaked particles, suggesting cardiomyocyte proliferation. While this method shows promise in targeting the infarct, it relies upon the upregulation of ICAM-1, which is a consequence of inflammation and is not solely cardiac-specific. To improve targeting capability, one can consider designing nanoparticle platforms that interact with biological signatures that are unique to the heart.

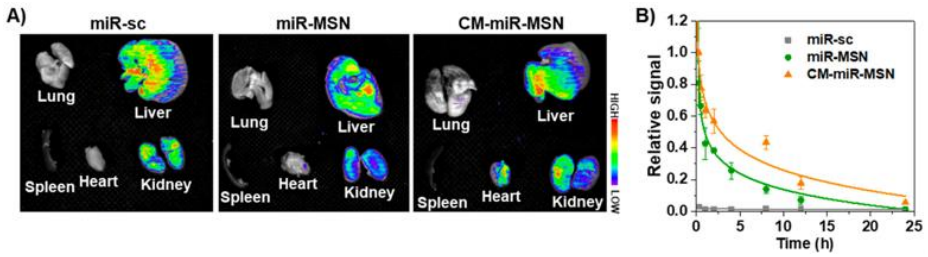


**Figure 1. 4: Improved localization of mesoporous silica nanoparticles (MSN) in the heart with the addition of cell membranes (CM).**
(A) Cy-3 labeled miRNA delivered using CM-modified MSNs resulted in higher accumulation in the heart compared to an MSN alone and a scrambled miR sequence (miR-sc). (B) CM-miR-MSN demonstrated enhanced blood circulation compared to controls. Reproduced from ref. 41 with permission from Elsevier, copyright 2020.

*1.2.2 Targeting protein and cellular features within the infarct*

To expand on inflammatory response targeting mechanisms that have been previously discussed, there is also a growing list of ways in which nanoparticle platforms are being designed to localize to features that are present in the heart. By incorporating multiple targeting moieties, Cheng et al. designed a "nanomatchmaker" comprised of an iron core that is capable of linking therapeutic cells to injured cells through the use of antibody conjugation to the nanoparticle surface ($95.7 \pm 14.5$nm)[43]. This platform (called MagBICE$_2$) uses anti-CD34 and anti-myosin light chain (MLC) antibodies to tether endogenous bone marrow derived stem cells (CD34) to injured cardiomyocytes (expressing MLC). Nanoparticles were IV injected 10 minutes after injury in a rat model of MI. To enhance nanoparticle targeting to the heart, some animals were subjected to a magnetic field that interacted with the nanoparticle's iron core. Animals were then harvested after 4 weeks to evaluate therapeutic efficacy. MagBICE$_2$ demonstrated significantly higher iron intensity and CD34$^+$ cells in the injured myocardium compared to animals treated with an iron nanoparticle control, Feraheme (FH). In addition, nanoparticle treatment increased the amount of viable tissue, as evaluated via Masson's trichrome, and improved left ventricular ejection fraction. These trends were further improved

when a magnetic field was applied to enhance nanoparticle localization. Magnetic field targeting further enhanced cardiac functional improvement over nanoparticle administration alone, demonstrating the utility of the iron core design. Overall, this platform is interesting in that the targeting moiety also acts as a mechanism for therapy, resulting in a simple but therapeutically efficient design. One can also see how this platform could be easily adapted to bear other antibodies, making it more versatile.

In vivo phage display is a technique that has emerged as a method for discovering tissue-specific targeting methods[44]. A phage library is injected in vivo and allowed to circulate for a certain amount of time at which point, the tissue of interest is collected, and the phages are isolated and amplified to be injected again. This process is repeated several times to isolate the phages that are known to localize to the site of interest. These phages can then be sequenced and used as targeting moieties. Kanki et al. completed this process for the ischemic left ventricle in a rat model of ischemia reperfusion with a Ph.D.-C7C phage library injected 10 minutes post-injury[45]. Three peptide motifs that demonstrated preferential binding to the ischemic myocardium compared to uninjured animals were identified. By conjugating these sequences to the recombinant fluorescent protein SUMO-mCherry, they assessed the affinity of each sequence to the ischemic myocardium and found that the sequence CSTSMLKAC localized best to the heart after MI. This sequence bears similarity to titin, a cytoskeletal protein that binds to alpha-B crystalline, thereby protecting titin from ischemic damage. Though the exact mechanism by which this peptide sequence targets is unknown, it is postulated that it is through interactions with alpha-B crystalline. This “cardiac homing peptide” sequence has been used to aid in targeting IV injection of exosomes to the infarcted heart 24 hours post-MI[46]. Both in vitro and in vivo, conjugation of the peptide sequence to exosomes was achieved through the use of a DOPE-NHS linker. When comparing the efficacy of exosomes conjugated to the cardiac homing peptide versus a scrambled peptide sequence,

there was a significantly higher ejection fraction and amount of viable myocardium in addition to decreased infarct size (**Figure 1.5**). Not only did the addition of a targeting peptide increase localization to the area of interest, it also allowed for a significant increase in cellular uptake of the exosomes, as demonstrated in vitro. The exploration of peptide sequences that target the heart has also been done by another group using an M13 phage library[47]. Using the same biopanning method of multiple rounds of injection, isolation, and amplification, they discovered the peptide sequence, APWHLSSQYSRT. Similar to the cardiac homing peptide, this sequence also shows improved localization and internalization in the heart in vivo and could also be used to aid in targeted therapeutic delivery to the heart.

During ischemic injury, the mitochondrial membrane is damaged in cardiomyocytes. This leads to mitochondrial dysfunction and, ultimately, cardiomyocyte death that is mediated by the opening of the mitochondrial pore complex in the inner mitochondrial membrane. Zhang et al.**[48]** developed lipid-polymeric nanoparticles that enable mitochondrial-targeted delivery of tanoshine IIA, a cardioprotective medicinal herb[49]. These lipid nanoparticles were modified with the triphenylphosphonium (TPP) cation to target mitochondria and D-$\alpha$-tocopheryl polyethylene glycol 1000 succinate (TPGS) to prolong blood circulation and enhance cellular uptake (~140nm in diameter). Following permanent occlusion of proximal left coronary artery, rats were injected via the tail vein every other day for 14 days. Targeted nanoparticles with the TPP cation showed significantly higher drug accumulation and reduced infarct size in the heart compared to non-targeted nanoparticle and free drug controls.

In another attempt to leverage the unique phenotype of mitochondria post-MI, Zhang et al. developed polyethylene glycol nanoparticles (54 nm) that had been modified with the Szeto-Schiller peptide sequence (SS31) to enable targeted delivery of Cyclosporin A (CsA), an immunosuppressive drug, to the heart after MI when administered via IV injection 5 minutes prior to reperfusion**[50]**. The SS31 sequence specifically localizes to the inner mitochondrial

membrane via interacting with cardiolipin. In vitro, increased cellular uptake of SS31-modified nanoparticles was demonstrated with hypoxia reoxygenated H9c2 cells. The damaged mitochondrial membrane enabled concentrated accumulation of SS31 particles and delivery of the therapeutic payload. In a rat model of acute MI, it was demonstrated that administration of nanoparticles loaded with CsA resulted in significantly less cellular apoptosis and reduced infarct size compared to CsA alone. This is an excellent example of how nanoparticles could be used to improve the bioavailability and efficacy of small molecule drugs. While this method of targeting works, it is not specific to only the heart; cardiolipin is found in the membranes of all mitochondria. Though mitochondrial damage is strongly present in the heart post-MI, it may not be exclusive to only the heart and platforms that are designed to target this abnormality could still be subject to off target effects.

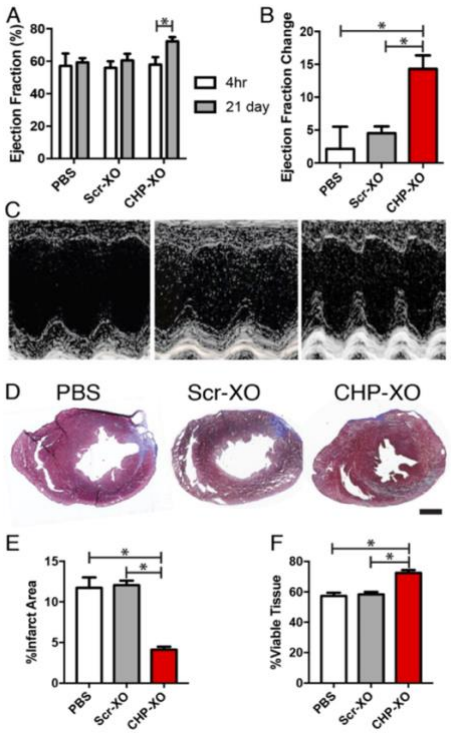


**Figure 1. 5: Exosomes (XO) modified with the cardiac homing peptide (CHP) improve heart function and reduce scar size.**
(A) CHP-XO treatment leads to ejection fraction improvement over time and (B) significant improvement compared to PBS and an exosome conjugated to a scrambled peptide sequence control (SCR-XO). (C) Representative M mode echocardiography images. (D) Masson's trichrome stained hearts show that CHP-XO treatment (E) decreases infarct area and (F) increases viable tissue. Reproduced from ref. 47 with permission from Ivyspring International Publisher, copyright 2018.

Targeting the angiotensin II type 1 ($AT_1$) receptor following MI has previously been shown to be a successful technique for directing nanoparticle delivery to the heart, as it is upregulated in the infarcted following MI[51]. By attaching an $AT_1$ targeting peptide to PEGylated dendrigraft poly-$_L$-lysine dendrimers (~50 nm), Xue et al. were able to deliver the anti-miR-1 antisense oligonucleotide to inhibit cardiomyocyte apoptosis[52]. One day post-MI, mice were injected with the dendrimer "nanovector" therapeutic or various controls via the tail vein. The nanovectors bearing the $AT_1$ targeting peptide demonstrated strong accumulation in the heart starting as soon as one-hour post-MI, as well as significantly reduced miR-1 expression compared to a non-targeted control. In addition, at 7 days post-MI there was a significant

reduction in TUNEL positive cells, indicating a reduction in cellular apoptosis, as well as a reduction in infarct size in response to treatment with the $AT_1$ receptor-targeted dendrimers. Having been used as a target for multiple nanoscale platforms, the $AT_1$ receptor appears to be a promising target for cardiovascular applications.

### 1.3 The future of targeted nanoscale platforms

The use of IV injection for administering therapeutics to the heart is simpler and more easily translatable than approaches that involve open-heart procedures or the use of catheter-based systems. The field of nanomedicine offers platforms that could be particularly applicable following MI. As customizable as these nanoscale platforms are, the main concern of IV injections, off target accumulation and reduced therapeutic efficacy, cannot be overlooked. To overcome this, methods for targeting the heart have been explored. As discussed, there are many different techniques for targeting—most center around leveraging the pathophysiology of the microenvironment of the infarcted heart. Common design criteria focus on interacting with the inflammatory response or proteins and cellular markers that are primarily found or upregulated in the heart. While these methods have proven successful in preclinical studies, they can still suffer from issues with off-target accumulation, as many of the targets are not solely unique to the heart. This is particularly problematic with systems that target hallmarks of the immune response as many of these features could allow for localization in other areas of inflammation. Patients with co-morbidities such as arthritis or cancer may not be eligible for platforms that are targeting upregulation of the immune response and hallmarks of inflammation. In addition, many NP platforms depend on the enhanced permeability of the tissue, which is only temporarily present in the infarcted heart[53], meaning the timeline for delivery is limited. As a result, many of these nanoparticle systems are only applicable for acute MI. Moreover, this permeability can go both ways, with materials struggling to be retained, unless targeting can be achieved via a morphological transition of the material[30]. To

advance nanomaterial therapeutic strategies, it could be beneficial to engineer nanoparticles that have a dual-targeting mechanism. Dual targeted mechanisms have been explored for other cardiovascular applications and have shown improved efficacy compared to single targeted counterparts[34, 54]. Nanoparticle platforms that are triggered by more than one stimulus have the potential to improve localization in the heart and are an area of nanomedicine research worth pursuing.

The use of targeting moieties to direct systemically injected therapeutics to the site of interest has been able to improve the therapeutic efficacy of various payloads loaded into nanoparticles or viral vectors, two types of nanoscale therapeutics. While therapeutic impact is the most important factor to consider, it is also crucial to assess the biodistribution of targeted therapeutics to ensure off target accumulation is mitigated. Though some of the examples discussed have included the necessary controls to demonstrate improvement over a non-targeted equivalent, there is still a need for more rigorous biodistribution quantification. With AAV delivery, PCR can be used to evaluate the transduction of various satellite organs. With administration of nanoparticle platforms, biodistribution methods are not standardized. Some nanoparticle platforms will be tagged with a fluorescent marker to allow for detection, however, the means for detecting these nanoparticles is highly variable. *In vivo* imaging system (IVIS) is a common method for measuring fluorescence in both living animals and excised tissues[55]. Other groups have adopted a homogenization method for detecting fluorescence in tissue samples[25, 56-58]. Overall, there is a need for the development of more standardized and high-resolution methods for detecting nanoparticle distribution in satellite tissues. This is particularly pertinent to platforms that claim targeting capability since there is currently a lack of quantitative biodistribution in the field.

For nanoparticle therapeutics, it is important to continue to explore new methods for targeting the heart. As discussed, there have been more efforts to increase cardiac-specific

targeting via *in vivo* phage display and surface modification with binding moieties such as RGD or $AT_1$ targeting peptides, but even these methods are not perfect and could benefit from added specificity.

Nanomedicine has become a powerful tool in cardiovascular research, allowing for improved circulation time and efficacy of systemically administered therapeutics in early preclinical studies. As the field evolves and grows, we can expect to see further improvements in mitigating off-target effects of therapeutic payloads through the clever use of physiological triggers and more cardiac-specific targets. Though the pathway to regulatory approval may be slower due to the increasing complexity in material design, it is worth the trade-off for optimized therapeutic impact. Additionally, as the field of targeted nanomedicine continues to expand, there is a need to continue to develop the field through incorporation of unique therapeutic moieties and exploration of particle morphology and biodistribution over time.

### 1.5 Thesis Outline

This thesis is divided into 5 chapters.

Chapter 1 investigates the use of targeted nanoscale particles and viral vectors for directing therapeutic delivery to the infarcted heart. When looking at the use of nanoparticle carriers in the heart, there are generally two main categories for selecting a target: utilizing a hallmark of the immune response or a tissue-specific feature of the injured myocardium. Viral vectors, on the other hand, rely more on tissue specific promoters. Overall, the use of targeted nanoscale therapeutics has become an increasingly relevant modality for treatment of acute myocardial infarction.

Chapter 2 introduces an MMP-responsive polynorbornene nanoparticle that bears a small molecule MMP-inhibitor. While this material has been previously established as a successful platform for targeting the infarcted heart, here we aimed to take this proof of

concept and turn it into a therapeutic. We hypothesized that this drug-loaded, MMP-responsive nanoparticle would be able to maintain the drug's bioactivity and successfully localize to the heart. This chapter demonstrates the feasibility of utilizing this nanoparticle platform for drug delivery in a model of acute myocardial infarction.

Chapter 3 expands upon the enzyme-responsive nanoparticle work by establishing a degradable nanoparticle system. Through modification of the polymer backbone via copolymerzation of norbornene with a low strain phosphoramidate containing cyclic olefin (MePTDO). Biodistribution comparison between this degradable platform and the material used in chapter 2 demonstrates distinct differences between the two. This chapter characterizes this degradable nanoparticle and demonstrates its ability to localize to the heart following enzymatic cleavage. Additionally, we show the clearance of this material over time out to 28 days post-injection in the heart and satellite organs.

Chapter 4 introduces a new polymeric material, an MMP-responsive protein-like polymer (PLP). Unlike the previous nanoparticle platforms, PLPs have a significantly lower molecular weight and therefore an amorphous, protein-like structure compared to forming spherical micelles. Here, we hypothesized that this new platform would exhibit significantly higher localization to the heart via enzyme cleavage due to its extended circulation half-life. This chapter characterizes this new material and demonstrates the localization and morphology of protein-like polymers in the heart over time. Additionally, *in vitro* studies for modeling cellular uptake of PLPs in inflammatory conditions.

The final chapter describes a summary of the results of this dissertation and significance of the presented work in nanomedicine research in the heart. Finally, the chapter suggests future studies for a deeper understanding of the mechanisms behind these

nanoscale platforms discussed here as well as potential therapeutic options to use with these systems.

### 1.6 Acknowledgements

I would like to acknowledge their funding sources NIH NHLBI R01HL139001 and R01HL113468. Additionally, I was supported by the Chemistry Biology Interfaces training grant (5T32GM112584) and the National Institutes of Health pre-doctoral fellowship (1F31HL152610-01).

Chapter 1 is part of a paper that has been published as a review paper in Biomaterials Science, Holly Sullivan, Nathan C. Gianneschi, Karen L. Christman. “Targeted nanoscale therapeutics for myocardial infarction”. The dissertation author was the first author of this papers.

## 1.7 References


1. M. A. Khan, M. J. Hashim, H. Mustafa, M. Y. Baniyas, S. Al Suwaidi, R. AlKatheeri, F. M. K. Alblooshi, M. Almatrooshi, M. E. H. Alzaabi, R. S. Al Darmaki and S. Lootah, *Cureus*, 2020, **12**, e9349.
2. Y. Birnbaum, M. C. Fishbein, C. Blanche and R. J. Siegel, *N Engl J Med*, 2002, **347**, 1426-1432.
3. V. Menon, J. G. Webb, L. D. Hillis, L. A. Sleeper, R. Abboud, V. Dzavik, J. N. Slater, R. Forman, E. S. Monrad, J. D. Talley and J. S. Hochman, *J Am Coll Cardiol*, 2000, **36**, 1110-1116.
4. R. Lemery, H. C. Smith, E. R. Giuliani and B. J. Gersh, *Am J Cardiol*, 1992, **70**, 147-151.
5. S. Pohjola-Sintonen, J. E. Muller, P. H. Stone, S. N. Willich, E. M. Antman, V. G. Davis, C. B. Parker and E. Braunwald, *Am Heart J*, 1989, **117**, 809-818.
6. B. S. Edwards, W. D. Edwards and J. E. Edwards, *Am J Cardiol*, 1984, **54**, 1201-1205.
7. T. D. Johnson and K. L. Christman, *Expert opinion on drug delivery*, 2013, **10**, 59-72.
8. M. D. Brown, R. Byyny, D. B. Diercks, S. R. Gemme, C. J. Gerardo, S. A. Godwin, S. A. Hahn, B. W. Hatten, J. S. Haukoos, G. S. Ingalsbe, A. Kaji, H. Kwok, B. M. Lo, S. E. Mace, D. J. Nazarian, J. A. Proehl, S. B. Promes, K. H. Shah, R. D. Shih, S. M. Silvers, M. D. Smith, M. E. W. Thiessen, C. A. Tomaszewski, J. H. Valente, S. P. Wall, S. J. Wolf, S. V. Cantrill, J. M. Hirshon, R. R. Whitson, T. Schulz, S. B. Promes, J. M. Glauser, M. D. Smith, S. S. Torbati and M. D. Brown, *Annals of Emergency Medicine*, 2017, **70**, 724-739.
9. L. A. Reis, L. L. Chiu, N. Feric, L. Fu and M. Radisic, *J Tissue Eng Regen Med*, 2016, **10**, 11-28.
10. A. A. Rane and K. L. Christman, *Journal of the American College of Cardiology*, 2011, **58**, 2615-2629.
11. S. Guo and L. Huang, *Biotechnol Adv*, 2014, **32**, 778-788.
12. L. F. de Oliveira, K. Bouchmella, A. Goncalves Kde, J. Bettini, J. Kobarg and M. B. Cardoso, *Langmuir*, 2016, **32**, 3217-3225.
13. I. Somasuntharam, A. V. Boopathy, R. S. Khan, M. D. Martinez, M. E. Brown, N. Murthy and M. E. Davis, *Biomaterials*, 2013, **34**, 7790-7798.
14. T. Bejerano, S. Etzion, S. Elyagon, Y. Etzion and S. Cohen, *Nano Lett*, 2018, **18**, 5885-5891.
15. F. Gao, M. Kataoka, N. Liu, T. Liang, Z. P. Huang, F. Gu, J. Ding, J. Liu, F. Zhang, Q. Ma, Y. Wang, M. Zhang, X. Hu, J. Kyselovic, X. Hu, W. T. Pu, J. Wang, J. Chen and D. Z. Wang, *Nat Commun*, 2019, **10**, 1802.
16. J. Bauersachs and J. D. Widder, *Pharmacol Rep*, 2008, **60**, 119-126.
17. L. Claesson-Welsh, *Upsala J Med Sci*, 2015, **120**, 135-143.
18. Y. Matsumura and H. Maeda, *Cancer Res*, 1986, **46**, 6387-6392.
19. H. Maeda, H. Nakamura and J. Fang, *Adv Drug Deliv Rev*, 2013, **65**, 71-79.
20. M. J. Johnston, S. C. Semple, S. K. Klimuk, S. Ansell, N. Maurer and P. R. Cullis, *Biochim Biophys Acta*, 2007, **1768**, 1121-1127.
21. H. L. Wong, R. Bendayan, A. M. Rauth, H. Y. Xue, K. Babakhanian and X. Y. Wu, *Journal of Pharmacology and Experimental Therapeutics*, 2006, **317**, 1372-1381.
22. A. C. Anselmo and S. Mitragotri, *Bioeng Transl Med*, 2016, **1**, 10-29.
23. M. Iafisco, A. Alogna, M. Miragoli and D. Catalucci, *Nanomedicine (Lond)*, 2019, **14**, 2391-2394.
24. A. C. Anselmo and S. Mitragotri, *Bioeng Transl Med*, 2019, **4**, e10143.

25. B. Semete, L. Booysen, Y. Lemmer, L. Kalombo, L. Katata, J. Verschoor and H. S. Swai, *Nanomedicine*, 2010, **6**, 662-671.
26. D. N. Granger, *Am J Physiol*, 1988, **255**, H1269-1275.
27. N. G. Frangogiannis, *Compr Physiol*, 2015, **5**, 1841-1875.
28. J. Simova, J. Skvor, D. Slovak, I. Mazura and J. Zvarova, *Folia Biol (Praha)*, 2013, **59**, 181-187.
29. R. C. Scott, J. M. Rosano, Z. Ivanov, B. Wang, P. L. Chong, A. C. Issekutz, D. L. Crabbe and M. F. Kiani, *FASEB J*, 2009, **23**, 3361-3367.
30. M. M. Nguyen, A. S. Carlini, M. P. Chien, S. Sonnenberg, C. Luo, R. L. Braden, K. G. Osborn, Y. Li, N. C. Gianneschi and K. L. Christman, *Adv Mater*, 2015, **27**, 5547-5552.
31. M. S. Lee, H. S. Park, B. C. Lee, J. H. Jung, J. S. Yoo and S. E. Kim, *Sci Rep*, 2016, **6**, 27520.
32. Z. Q. Dong, J. Guo, X. W. Xing, X. G. Zhang, Y. M. Du and Q. H. Lu, *Biomed Pharmacother*, 2017, **89**, 297-304.
33. A. Abuchowski, J. R. McCoy, N. C. Palczuk, T. van Es and F. F. Davis, *J Biol Chem*, 1977, **252**, 3582-3586.
34. R. Zhang, R. Liu, C. Liu, L. Pan, Y. Qi, J. Cheng, J. Guo, Y. Jia, J. Ding, J. Zhang and H. Hu, *Biomaterials*, 2019, DOI: 10.1016/j.biomaterials.2019.119605, 119605.
35. Y. Gao, X. Wang and C. He, *J Ethnopharmacol*, 2016, **193**, 524-530.
36. B. Sun, S. Liu, R. Hao, X. Dong, L. Fu and B. Han, *Pharmaceutics*, 2020, **12**.
37. D. Ji, Q. Wang, Q. Zhao, H. Tong, M. Yu, M. Wang, T. Lu and C. Jiang, *J Nanobiotechnology*, 2020, **18**, 86.
38. L. P. Ganipineni, B. Ucakar, N. Joudiou, R. Riva, C. Jérôme, B. Gallez, F. Danhier and V. Préat, *J Drug Target*, 2019, **27**, 614-623.
39. G. Zheng, M. Zheng, B. Yang, H. Fu and Y. Li, *Biomed Pharmacother*, 2019, **116**, 109006.
40. C. Yao, W. Wu, H. Tang, X. Jia, J. Tang, X. Ruan, F. Li, D. T. Leong, D. Luo and D. Yang, *Biomaterials*, 2020, **257**, 120256.
41. H. W. M. Niessen, W. K. Lagrand, C. A. Visser, C. J. L. M. Meijer and C. E. Hack, *Cardiovascular Research*, 1999, **41**, 603-610.
42. G. L. Kukielka, H. K. Hawkins, L. Michael, A. M. Manning, K. Youker, C. Lane, M. L. Entman, C. W. Smith and D. C. Anderson, *J Clin Invest*, 1993, **92**, 1504-1516.
43. K. Cheng, D. Shen, M. T. Hensley, R. Middleton, B. Sun, W. Liu, G. De Couto and E. Marbán, *Nature Communications*, 2014, **5**, 4880.
44. G. P. Smith, *Science*, 1985, **228**, 1315-1317.
45. S. Kanki, D. E. Jaalouk, S. Lee, A. Y. Yu, J. Gannon and R. T. Lee, *J Mol Cell Cardiol*, 2011, **50**, 841-848.
46. A. Vandergriff, K. Huang, D. Shen, S. Hu, M. T. Hensley, T. G. Caranasos, L. Qian and K. Cheng, *Theranostics*, 2018, **8**, 1869-1878.
47. M. Zahid, B. E. Phillips, S. M. Albers, N. Giannoukakis, S. C. Watkins and P. D. Robbins, *PLoS One*, 2010, **5**, e12252.
48. S. Zhang, J. Li, S. Hu, F. Wu and X. Zhang, *Int J Nanomedicine*, 2018, **13**, 4045-4057.
49. X. Yuan, S. Jing, L. Wu, L. Chen and J. Fang, *Exp Ther Med*, 2014, **8**, 973-977.
50. C. X. Zhang, Y. Cheng, D. Z. Liu, M. Liu, H. Cui, B. L. Zhang, Q. B. Mei and S. Y. Zhou, *J Nanobiotechnology*, 2019, **17**, 18.
51. T. Dvir, M. Bauer, A. Schroeder, J. H. Tsui, D. G. Anderson, R. Langer, R. Liao and D. S. Kohane, *Nano Lett*, 2011, **11**, 4411-4414.
52. X. Xue, X. Shi, H. Dong, S. You, H. Cao, K. Wang, Y. Wen, D. Shi, B. He and Y. Li, *Nanomedicine*, 2018, **14**, 619-631.

53. L. D. Horwitz, D. Kaufman, M. W. Keller and Y. Kong, *Circulation*, 1994, **90**, 2439-2447.
54. B. Banik, B. Surnar, B. Askins, M. Banerjee and S. Dhar, *ACS Appl Mater Interfaces*, 2019, DOI: 10.1021/acsami.9b19036.
55. J. Kennedy, E. Larraneta, M. T. C. McCrudden, C. M. McCrudden, A. J. Brady, S. J. Fallows, H. O. McCarthy, A. Kissenpfennig and R. F. Donnelly, *J Control Release*, 2017, **265**, 57-65.
56. D. J. Castro, S. Haghighat, R. E. Saxton, E. Reisler, N. Jongwaard, D. J. Castro, P. H. Ward and R. B. Lufkin, *Laryngoscope*, 1992, **102**, 868-874.
57. Y. Y. Cheng and T. H. Tsai, *J Agric Food Chem*, 2017, **65**, 1078-1085.
58. F. Meng, J. Wang, Q. Ping and Y. Yeo, *ACS Nano*, 2018, **12**, 6458-6468.

## Chapter 2: Enzyme-Responsive Nanoparticles for the Targeted Delivery of an MMP Inhibitor to the Heart post Myocardial Infarction

### 2.1 Introduction

Myocardial infarction (MI) is the leading cause of global deaths,[1] as mentioned in chapter one, this leads to ischemic damage and cardiomyocyte death. During acute ischemic injury, there is enhanced vascular permeability and retention, or "leaky vasculature", in the infarct. In addition to this, an upregulation of inflammatory enzymes such an matrix metalloproteinases (MMPs) begin to degrade the native extracellular matrix (ECM) within the heart, compromising mechanical support in addition to cardiomyocyte structure and function.[2] MMP activity is upregulated within hours post-MI and can remain at high levels for weeks to months afterwards.[3] Despite the current standard-of-care, over time, ischemic tissue damage leads to negative left ventricle (LV) remodeling[4], including LV dilation and wall thinning, and eventual heart failure in many patients[5].

MMP inhibition by systematic administration of pharmacological MMP inhibitors (MMPi) has shown promise in attenuating LV dilatation and reducing infarct size in MI and heart failure models.[6-8] However, these drugs face challenges upon clinical translation. First, many of these molecules have poor water solubility and short half-lives (24~48 hours post administration), and are unable to achieve effective inhibitory concentration in the infarcted heart.[8, 9] Second, repetitive dosing and non-targeted systemic delivery has led to off-target side effects, such as joint pain and stiffness associated with musculoskeletal syndrome.[10, 11] To address these problems, hydrogels have been used as controlled delivery platforms for MMPi biologics[12, 13] to improve targeting. The advantages of hydrogels include good targeting and potential long-term retention in the infarct. However, the requirement of injection directly into the injured myocardium prevents their use during the acute phase of MI, given the risk of cardiac rupture.[14, 15]

As previously mentioned in chapter 1, nanoparticle-based therapeutics are an alternative delivery platform that can be administrated via minimally invasive intravenous (IV) injection and extravasate into the infarct through the highly permeable vasculature present acutely post-MI.[16, 17] Active targeting can also be achieved through nanoparticle surface functionalization, such as incorporating substrates for upregulated angiotensin-1 receptor[18, 19], P-selectin[20], and various mitochondrial targets[21, 22]. Despite this, nanoparticles still face the risk of fast clearance (within hours to days post-injection) due to leakage from the infarct and opsonization, wherein biomolecules occlude the surface of particles and subsequently inhibit interaction with tissue receptors.[23] In light of this, a drug delivery platform that can be administered minimally invasively and then selectively accumulate in the infarct for long-term retention is highly desirable.

Our group developed MMP-responsive nanoparticles that successfully targeted and were retained in the infarcted heart for up to 28 days following systematic administration by undergoing a morphological switch from nanoparticles to micron scale aggregates, as discussed in chapter 1.[24] These materials were made from peptide-polymer amphiphiles where an inert hydrophobic block was followed by a hydrophilic block of MMP-2/MMP-9 cleavable peptides. Following IV injection, these nanoparticles exited the leaky vasculature and were physically trapped in the infarcted region of the heart due to MMP-induced peptide cleavage, which altered the hydrophilic to hydrophobic ratio, and subsequent material aggregation **(Scheme 1)**. This MMP-directed active assembly prevented the material from leaking out into the blood stream, enabling long-term retention.

In this work, we aimed to turn this proof of concept study into a therapeutic platform by conjugating a small molecule MMPi drug, PD166793,[7] to the polymer backbone for enhanced delivery and therapeutic retention in the infarct. PD166793 has been shown to significantly

reduced MMP activity and LV dilation while preserving systolic function in a porcine MI model,[25] but the requirement of repeated oral dosing to achieve a therapeutic outcome[26] in combination with its poor water solubility have prevented its use in clinical trials[7]. We hypothesized that packaging this drug into our enzyme-responsive nanoparticles would allow for targeted delivery to the infarct. When micellar nanoparticles form, the drug will be shielded in the core, then exposed and released following aggregation after enzymatic cleavage of the hydrophilic peptide. As a first step towards the development of this therapeutic, in this study, we set out to determine whether conjugation of PD166793 to the MMP responsive nanoparticles would still allow for enzyme mediated aggregation *in vitro* and *in vivo*, and whether the drug would be released and remain active.

### 2.2 Results

*2.2.1 Norbornene monomer (NorMMPi) serves as a prodrug and bioactive PD166793 can be released via proteolysis.*

Yifei Liang at Northwestern University first synthesized the MMP inhibitor (MMPi) PD166793 and its functionalized norbornene monomer (NorMMPi). Their inhibitory effects against MMPs were examined using an MMP activity assay. For the control groups, 100% peptide cleavage was observed post DMSO treatment, and no cleavage was detected after EDTA treatment (**Figure S4**). While free PD166793 blocked 70% of MMP activity, no MMP inhibition was observed upon the NorMMPi treatment. This result indicates that NorMMPi serves as a prodrug by shielding the carboxylic acid from interaction with MMP catalytic center, which agrees well with the previous reported drug mechanism of action.[7] To confirm the bioactive PD166793 can be released from NorMMPi via ester bond cleavage, an esterase mediated proteolysis assay was used. PD166793 has a strong UV absorbance at 270 nm, which enabled us to monitor its release via HPLC (**Figure S5**). While NorMMPi showed good stability in buffer and did not display any HPLC signal under

the running condition, we observed complete PD166793 release after 24 hours of incubation with esterase at 37 °C. This result suggests that the drug in the nanoparticle core should be amenable for release upon exposure to the enzyme-rich infarct microenvironment after MMP-induced aggregation.

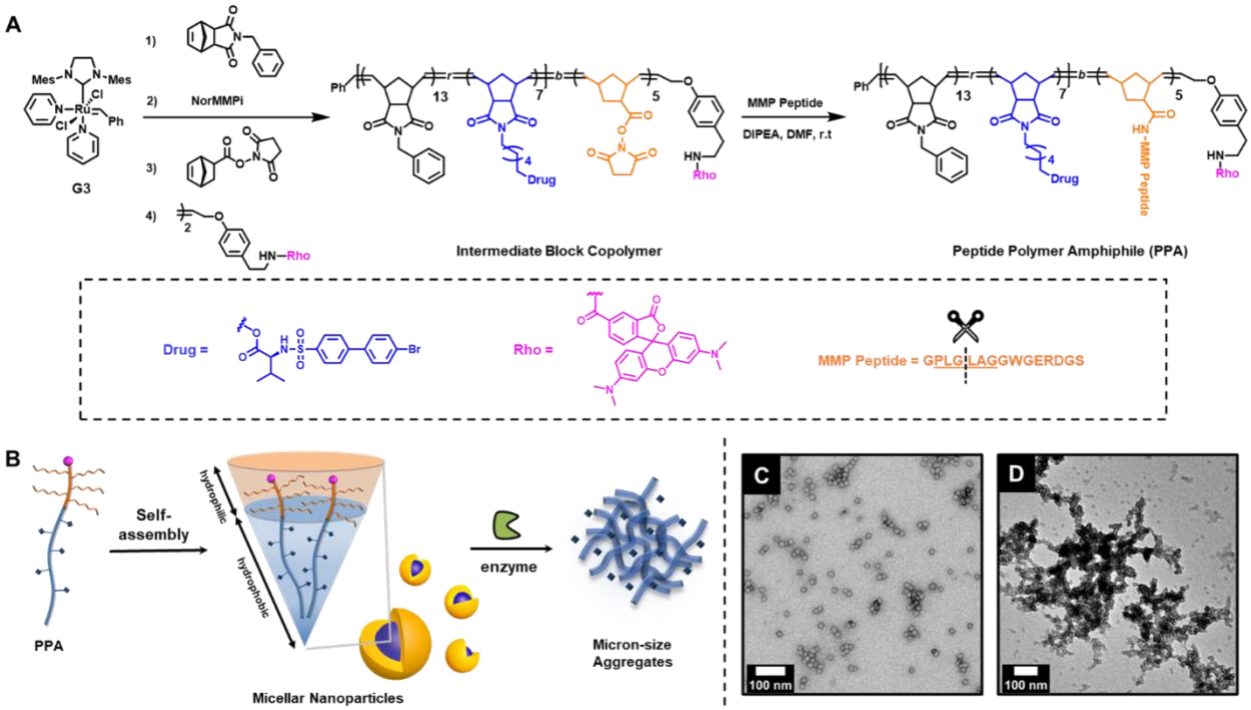


**Figure 2. 1: Synthesis of PD166793 loaded nanoparticles and enzyme-induced morphology switch.**

(A) Synthesis of PD166793 loaded peptide-polymer amphiphiles (PPAs). (B) Schematic demonstration for PPA self-assembly into nanoparticles and the enzyme-induced microscale aggregates formation. Transmission electron microscopy images of (C) nanoparticles and (D) aggregates formation post thermolysin treatment. (Figure generated by Yifei Liang)

*2.2.2 PD166793 loaded nanoparticles maintain enzyme responsiveness (Performed by Yifei Liang)*

PD166793 loaded peptide-polymer amphiphiles (PPAs) (20% wt% drug) were prepared (**Figure 1A**). The degree of polymerization (DP) of each block was optimized, targeting a ratio of 13:7 phenyl-norbornene (NorPh) to NorMMPi to provide a PD166793 plasma level (assuming 100% drug release post 300 nmol PPA injection in the rat model) similar to the effective concentration of 100 µmol/L.[24, 27] Calculations can be found in Supporting Information.

By solvent switch from DMSO to DPBS buffer, PPAs assembled into spherical micelles with a diameter of 15 nm as visualized by TEM (**Figure 1B-C**). To examine the enzyme responsiveness, the nanoparticles (NPs) were incubated with thermolysin at 37 °C in DPBS buffer (1 µM thermolysin: 100 µM polymer). Both TEM analysis (**Figure 1D**) and DLS measurement confirmed an enzyme-induced morphological switch from nanoparticles to microscale assemblies. Through this *in vitro* analysis, we showed that the PD166793-loaded nanoparticles maintained enzyme responsiveness.

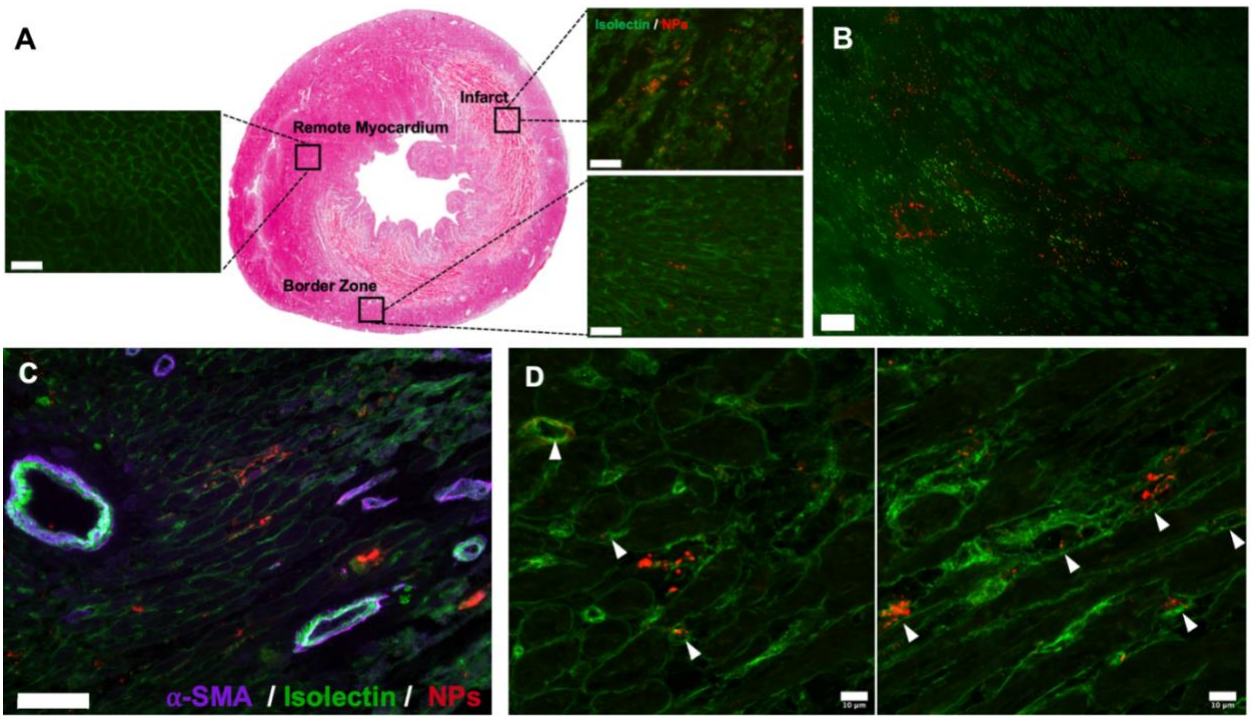


**Figure 2. 2: MMPi NPs localize to the infarct and extravasate from leaky vasculature**
**(A**) Following IV injection, rhodamine-labeled MMPi NPs localized to the infarct with no accumulation in the remote myocardium. **(B)** At 7 days post-injection, MMPi NPs are still present in the infarct. **(C)** MMPi NPs do not obstruct large vessels (scale bar: 100μm). **(D)** Confocal imaging shows a combination of extracellular deposition of MMPi NPs as well as some aggregate formation within the endothelial cell layer in capillaries (identified by white arrows).

*2.2.3 MMPi NPs localize to the infarct in rat acute MI model*

After administration via IV injection, MMPi NPs were visualized in the heart using fluorescence microscopy. As was previously observed with non-drug loaded NPs, MMPi NPs were found to accumulate in the infarcted region of the left ventricle with a majority of the aggregates in the infarct rather than the borderzone (**Figure 2A**).[24] No MMPi NPs or aggregates were observed in the remote myocardium (septum) or right ventricle. This result is consistent with the non-drug loaded NPs[24] and demonstrates retained regioselectivity of accumulated NPs in the heart. Like in our previous studies[24], MMPi NPs were still visible in the heart at 7 days post-injection (**Figure**

**2B**). At 7 days, we also evaluated the presence of macrophages as an initial evaluation of biocompatibility showing no differences compared to a saline injection (**Figure S7**).

*2.2.4 NP aggregates form in the infarct tissue and not in vasculature*

The proposed mechanism of aggregation and accumulation of this platform involves extravasation of nanoparticles from the leaky vessels in the heart post-acute MI. MMPi NPs then will encounter extracellular MMPs and undergo peptide cleavage and accumulation. To confirm localization, smooth muscle cells and endothelial cells were stained with alpha-smooth muscle actin (α-SMA) and isolectin for visualization. MMPi NPs were mostly found outside of the vasculature; fluorescence microscopy images revealed that MMPi NPs do not block arterioles (**Figure 3C**). Through confocal microscopy, we observed MMPi NPs aggregation in the extracellular space as well as in the endothelial layer of some capillaries, which could be attributed to the premature aggregation caused by the MMP released from the endothelial cells[28] (**Figure 3D**).

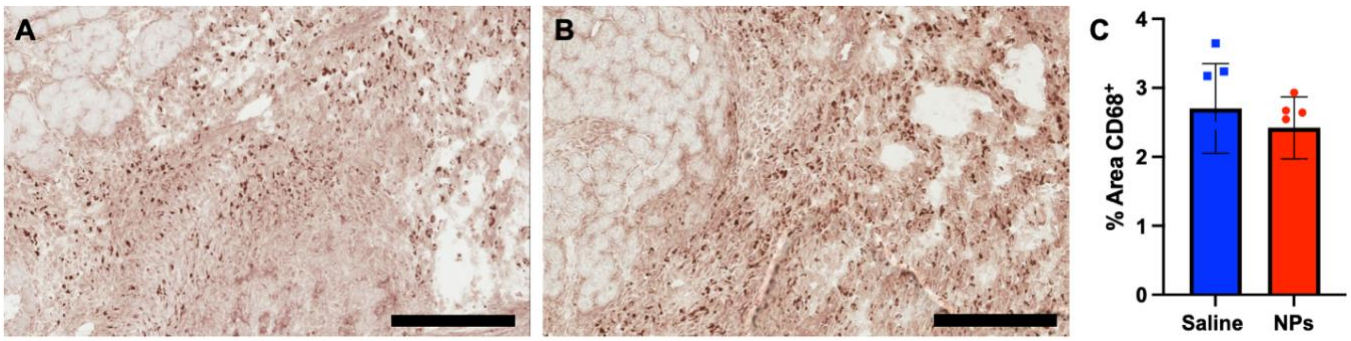


**Figure 2. 3: MMPi NPs to not increase macrophage recruitment to the heart**
CD68 staining in the infarct at 7 days post-injection show no sign of increased macrophage presence when comparing the the saline-injected (A) or nanoparticle-injected (B) hearts (scale bar: 200 μm). (C) Quantification of these images confirms this trend.

*2.2.5 Macrophage density is not impacted by nanoparticle administration.*

In animals harvested at 7 days post-MI, heart sections were stained for macrophages (**Figure 3A and B**). We observed no significant differences in macrophage density between saline and MMPi

NP treated animals (**Figure 3C**). This allows us to conclude that our MMPi NPs did not increase recruitment of macrophages into the infarcted region.

*2.2.6 Maximally loading PD166793 does not affect nanoparticle enzyme responsiveness and morphology transition*

After confirming that PD166793 loaded **NP** are enzyme responsive and can target infarcted myocardium, we next wanted to examine whether maximally loading PD166793 would affect nanoparticle size and the morphology transition to micron scale aggregates**. $PPA_{Max}$** with a DP of 20:5 (NorMMPi:peptide) was synthesized (**Figure S6A**) as described above and formulated into particles **$NP_{Max}$** (**Figure 4A**). As compared to the original MMPi NPs (20% wt% drug), the drug loading was increased to 40% wt% for **$NP_{Max}$** (detailed calculation in Supporting Information). An inert **$PPA_C$** without drug incorporation (NorPh: peptide = 20: 5) was also prepared as a control (**Figure S6B**) and assembled into spherical micelles **$NP_C$** (**Figure 4C**). Both NPs underwent aggregation upon thermolysin treatment (**Figure 4B** and **4D**). TEM analysis revealed that both **$NP_{Max}$** and **$NP_C$** had similar sizes as the original NPs (15~20 nm in diameter) and similarly underwent thermolysin induced aggregation to form micro-scale assemblies (**Figure 4B** and **4D**).

*2.2.7 Maximally loaded PD166793 nanoparticles are cytocompatible and bioactive*

With the fully loaded MMPi **$NP_{Max}$**, we next wanted to evaluate the cytocompatibility of this platform. It has been previously postulated that ~10% of the injected NPs accumulate in the infarcted region of the heart. In addition, the circulating concentration of MMPi NPs following injection will be ~18 μM under the assumption that each rat has a total blood volume of 16 mL. This provided us with target concentrations of relevance for our studies. Results from an alamarBlue™ assay show that the concentrations of NPs tested did not significantly alter L929

metabolic activity compared to a positive PBS control up to 41 μM (**Figure 4E**). This result demonstrates preliminary safety of our drug-loaded NP platform.

When treated with equivalent concentrations of MMPi $\mathbf{NP_{Max}}$ and free MMPi, we observed a significant improvement in cell metabolic activity for the former at high drug concentrations (75-1200 μM) (**Figure 4F**). This drug concentration correlates to a NP concentration of ranging from 60 to 3.75 μM, the aforementioned physiologically relevant concentration of MMPi NPs in the body and infarcted region. This suggests that a higher dose of PD166793 may be safely tolerated when it is conjugated to the polymeric backbone.

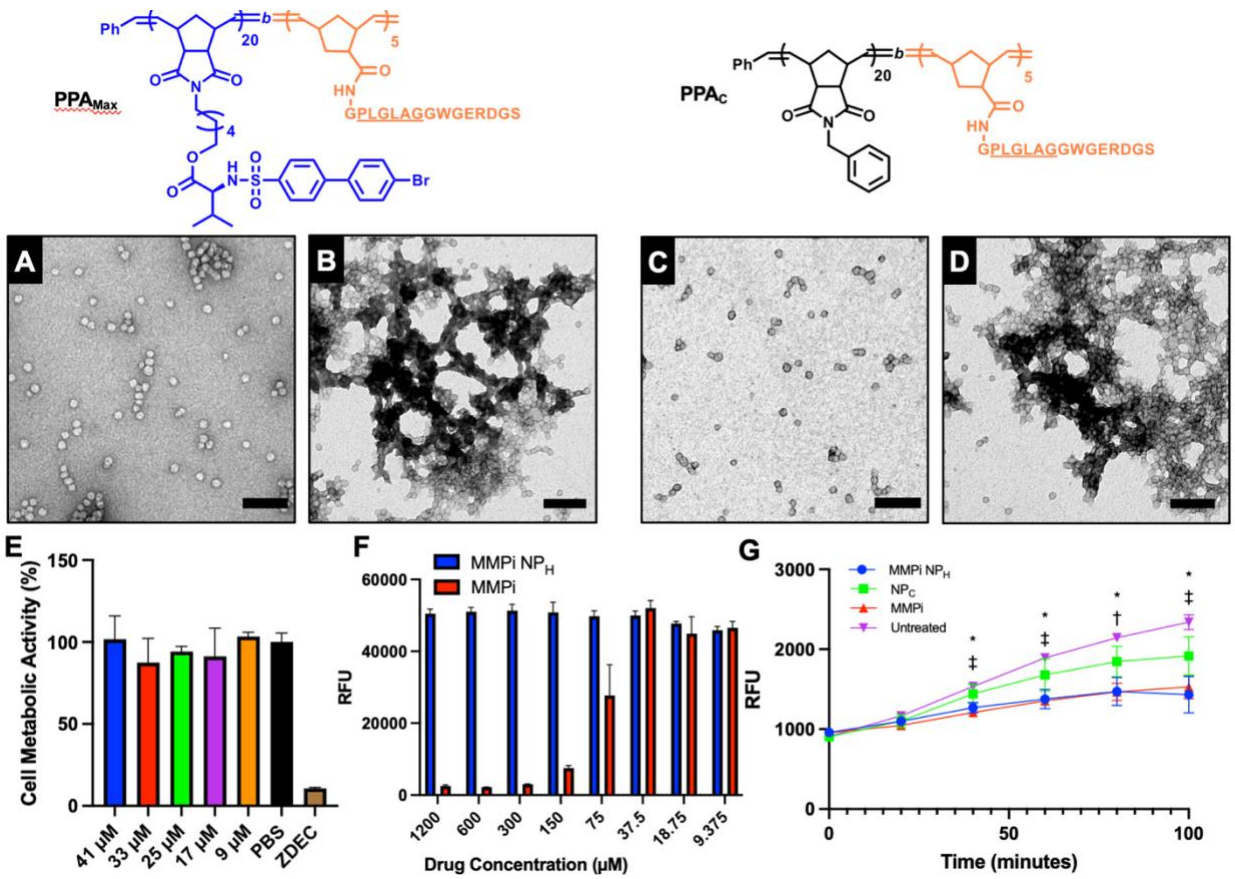


**Figure 2. 4: MMPi NP$_{Max}$ and empty NPC are enzymatically responsive and MMPi NPs are cytocompatible and maintain drug bioactivity.**
Max drug loaded **PPA$_{Max}$** and control **PPA$_C$** polymers still form micellar NPs **(A)** and **(C)** of the same size as the initial PD166793 **NP**. Additionally, both still form micron-scale aggregate structures after incubation with thermolysin **(B)** and **(D)**. **(E)** MMPi **NP$_{Max}$** does not significantly impact metabolic activity via alamarBlue™ assay. **(F)** Treatment of L929s with free drug (MMPi) results in reduced metabolic activity at high concentrations whereas conjugated drug (MMPi **NP$_{Max}$**) appears to offer a protective effect. **(G)** MMP activity is significantly decreased when treated with MMPi, MMPi **NP$_{Max}$**, and even **NP$_C$** compared to an untreated control (*P < 0.05 MMPi **NP$_{Max}$** compared to untreated, †P < 0.05 MMPi compared to untreated, ‡P < 0.001 MMPi compared to untreated via 2-way ANOVA with Tukey's post-hoc test). (Panels A-D generated by Yifei Liang)

Finally, we sought to confirm the bioactivity of the small molecule MMPi conjugated to the polymer backbone in the fully loaded nanoparticles. In a time-course experiment, we observed that both

MMPi **$NP_{Max}$** and free MMPi were capable of significantly inhibiting MMP activity within 40 minutes of incubation compared to a PBS control by 17.4% and 21.3% respectively (**Figure 4G**). From this, we can conclude that packaging the small molecule drug does not negatively impact the bioactivity of PD166793 and that there is rapid drug release from MMPi **$NP_{Max}$**.

### 2.3 Discussion

We have developed a novel enzyme-responsive nanoparticle therapeutic for the potential treatment of acute myocardial infarction (MI). Using ROMP, different dosages of a small molecule MMP inhibitor PD166793 can be incorporated into peptide-polymer amphiphiles though a hydrolysable ester linkage, and subsequently into the core of micellar nanoparticles.

Using a rat MI model, we found that MMPi NPs were able to successfully localize to the infarcted region of the heart following IV injection. Similarly, to the non-drug loaded platform, we observed that MMPi NPs are regiospecific with high accumulation in the infarct, some in the border zone, and little to no accumulation in the remote myocardium. Additionally, these NPs showed prolonged retention in the heart, with aggregates still visible at 7 days post injection. NP retention for this extended window could allow for maximal drug release over time.

In our initial design, we hypothesized that MMP-responsive NPs were extravasating from leaky vasculature in the infarct. Here, we were able to show that arterioles are not occluded by rhodamine-labeled MMPi **$NP_{Max}$**. Upon inspection of smaller capillaries using confocal imaging, we observed some nanoparticle presence within the endothelial layer. However, we also see MMPi **$NP_{Max}$** aggregates in the extracellular space. Since it has been previously established that endothelial cells express MMPs,[28] it is not surprising to observe MMPi **$NP_{Max}$** presence in the capillary endothelium. This could also have therapeutic relevance in inhibiting MMP presence at

this location. As further safety evidence, we observed no increase in macrophage presence in the infarct in both saline and MMPi **$NP_{Max}$** -treated animals.

To demonstrate the feasibility of maximally loading PD166793 (**$NP_{Max}$**), we first assessed their cytocompatibility *in vitro*. We observed that when the small molecule MMP-inhibitor is conjugated to the polymer backbone, it is tolerated by cells at significantly higher concentrations compared to a comparable concentration of free drug. This is because the drug is not bioactive until it is cleaved from the polymer backbone by endogenous esterase, leading to a slower sustained release of drug compared to a burst release.

When assessing biological activity, we observed equivalent MMP-inhibition by both the MMPi **$NP_{Max}$** and free MMPi *in vitro.* This allows us to conclude that the drug is successfully being released from the polymer backbone and is still bioactive and maintains therapeutic efficacy. Additionally, the comparable onset of inhibition from both MMPi **$NP_{Max}$** and free MMPi implies that the drug release from the polymer backbone is rapid, which could be beneficial for quick therapeutic delivery during the acute phase of MI. Knowing that the drug is still bioactive and that a higher dose may be tolerable when conjugated to the polymer backbone, it is possible that by utilizing our NP platform could allow for safe delivery of high concentrations of PD166793, thus mitigating the need for excessive repeat doses.

This study demonstrates initial proof of concept for the conjugation of a MMPi to MMP responsive nanoparticles. Since any therapeutic that is amenable for chemical conjugation can be included as monomer, we envision this targeted NP platform to be a generalizable approach for drug delivery and the treatment of other inflammatory diseases.

## 2.4 Methods

*In vitro enzyme-induced aggregation*

MMPi nanoparticles (NPs) (100 μM, with respect to polymer) were treated with thermolysin, an MMP alternative with improved thermostability, (1 μM) or DPBS for 24 hours at 37 °C in 1X DPBS. The resulting nanoparticle solutions were analyzed by dynamic light scattering (DLS) (**Figure S3**) and transmission electron microscopy (TEM) (**Figure 2C-D**) to examine the change in morphology. For the TEM samples, 5 μL of sample was applied to a 400-mesh carbon grid (Ted Pella, Inc.) that had been glow discharged for 15 seconds. 5 μL of 2 wt.% uranyl acetate solution was then applied and wicked away post 30 sec for staining.

*Surgical procedures and IV injection*

All procedures in this study were approved by the Committee on Animal Research at the University of California, San Diego and the Association for the Assessment and Accreditation of Laboratory Animal Care. Female, Sprague Dawley rats (225 – 250g) underwent ischemia-reperfusion (IR) procedures via left thoracotomy and temporary occlusion of the left anterior descending artery for 35 minutes.[23] One day post-MI, animals were anesthetized using isoflurane and arbitrarily assigned to IV injection of either 1 mL of MMPi NPs (300μM) or saline and harvested at one day (n = 2) or 6 days (n = 3) post-injection. Animals were euthanized via overdose of pentobarbital (200 mg/kg) and the heart, kidney, spleen, lungs, and liver were collected for histological analysis.

*Histology and immunohistochemistry*

Following euthanasia, hearts were dissected and fresh frozen in OCT for cryosectioning. Hearts were stained with hematoxylin and eosin to visualize the infarcted region of the heart. Slides

were scanned on an Aperio ScanScope CS2 brightfield slide scanner. Additional heart sections were stained with anti-α-SMA (1:75 dilution, Dako) and Alexa Fluor-647 (1:500 dilution, ThermoFisher) and isolectin (1:75 dilution, Vector Laboratories) to visualize large arterioles and capillaries.

*Cytocompatibility of MMPi NPs and free MMPi*

Murine fibroblast cells (L929) were seeded into a 96 well plate and left to adhere overnight. Following cell adhesion, MMPi **$NP_{Max}$** were diluted with sterile PBS to generate concentrations ranging from 41 to 9 µM and were added to the media with PBS and zinc diethyldithiocarbamate (ZDEC) at a concentration of 47mM serving as positive and negative controls, respectively. Treated cells were then incubated for 24 hours before performing an alamarBlue™ assay to evaluate their metabolic activity.

To compare the cytocompatibility of MMPi NPs and free MMPi, L929s were again plated and allowed to adhere overnight. Cells were then treated with MMPi **$NP_{Max}$** or an equivalent concentration of free MMPi ranging from 1200 to 9.375µM. PBS was used as a positive control and DMSO was used to control for the solvent used to dissolve the free drug. After 24 hours of treatment incubation, an alamarBlue™ assay was run on treated cells to evaluate their metabolic activity.

*Assessment of MMP activity in vitro*

Adherent murine fibroblasts (L929s) were plated and allowed to adhere overnight in a 96 well plate at a seeding density of 16,000 cells/well. Media from the plated cells was collected and treated with either MMPi **$NP_{High}$** (14.28 µM with respect to polymer, 285 µM with respect to drug), free MMPi (285 µM), PBS, or DMSO. The free drug concentration was calculated to

match that loaded in the **$NP_{High}$**. Following 20 minutes of treatment, an MMP-cleavage fluorescent FRET peptide (Amplite™) was added to track MMP activity over time following the manufacturer's instructions. The plate was then incubated at 37 °C and data points were taken every 20 minutes for 3 hours.

### 2.5 Acknowledgements

The authors would like to acknowledge their funding sources 1R01HL139001, additionally HLS was supported by F31 HL152610-03. We would like to acknowledge the Stem Cell and Genomics core in the Sanford Consortium for Regenerative Medicine for use of their microscopes.

Chapter 2 is currently being prepared for submission for publication of the material, Holly Sullivan, Yifei Liang, Kendra Worthington, Colin Luo, Nathan C. Gianneschi, Karen L. Christman. "Enzyme-Responsive Nanoparticles for the Targeted Delivery of an MMP Inhibitor to the Heart post Myocardial Infarction". The dissertation author is the co-first author of this paper.

## 2.6 References


1. E. J. Benjamin, P. Muntner, A. Alonso, M. S. Bittencourt, C. W. Callaway, A. P. Carson, A. M. Chamberlain, A. R. Chang, S. Cheng, S. R. Das, F. N. Delling, L. Djousse, M. S. V. Elkind, J. F. Ferguson, M. Fornage, L. C. Jordan, S. S. Khan, B. M. Kissela, K. L. Knutson, T. W. Kwan, D. T. Lackland, T. T. Lewis, J. H. Lichtman, C. T. Longenecker, M. S. Loop, P. L. Lutsey, S. S. Martin, K. Matsushita, A. E. Moran, M. E. Mussolino, M. O'Flaherty, A. Pandey, A. M. Perak, W. D. Rosamond, G. A. Roth, U. K. A. Sampson, G. M. Satou, E. B. Schroeder, S. H. Shah, N. L. Spartano, A. Stokes, D. L. Tirschwell, C. W. Tsao, M. P. Turakhia, L. B. VanWagner, J. T. Wilkins, S. S. Wong, S. S. Virani, E. American Heart Association Council on, C. Prevention Statistics and S. Stroke Statistics, *Circulation*, 2019, **139**, e56-e528.
2. V. L. Roger, *Med. Clin. North Am.*, 2007, **91**, 537-552; ix.
3. C. S. Webb, D. D. Bonnema, S. H. Ahmed, A. H. Leonardi, C. D. McClure, L. L. Clark, R. E. Stroud, W. C. Corn, L. Finklea, M. R. Zile and F. G. Spinale, *Circulation*, 2006, **114**, 1020-1027.
4. M. G. S. J. Sutton and N. Sharpe, *Circulation*, 2000, **101**, 2981-2988.
5. B. A. French and C. M. Kramer, *Drug Discov Today Dis Mech*, 2007, **4**, 185-196.
6. D. Vanhoutte, M. Schellings, Y. Pinto and S. Heymans, *Cardiovasc. Res.*, 2006, **69**, 604-613.
7. N. Kaludercic, M. L. Lindsey, B. Tavazzi, G. Lazzarino and N. Paolocci, *Cardiovasc Ther*, 2008, **26**, 24-37.
8. F. G. Spinale, *Physiol Rev*, 2007, **87**, 1285-1342.
9. W. M. Yarbrough, R. Mukherjee, G. P. Escobar, J. T. Mingoia, J. A. Sample, J. W. Hendrick, K. B. Dowdy, J. E. McLean, A. S. Lowry, T. P. O'Neill and F. G. Spinale, *Circulation*, 2003, **108**, 1753-1759.
10. K. Li, F. R. Tay and C. K. Y. Yiu, *Pharmacol Ther*, 2020, **207**, 107465.
11. M. P. Hudson, P. W. Armstrong, W. Ruzyllo, J. Brum, L. Cusmano, P. Krzeski, R. Lyon, M. Quinones, P. Theroux, D. Sydlowski, H. E. Kim, M. J. Garcia, W. A. Jaber and W. D. Weaver, *J. Am. Coll. Cardiol.*, 2006, **48**, 15-20.
12. B. P. Purcell, D. Lobb, M. B. Charati, S. M. Dorsey, R. J. Wade, K. N. Zellars, H. Doviak, S. Pettaway, C. B. Logdon, J. A. Shuman, P. D. Freels, J. H. Gorman, 3rd, R. C. Gorman, F. G. Spinale and J. A. Burdick, *Nat Mater*, 2014, **13**, 653-661.
13. Z. Fan, M. Fu, Z. Xu, B. Zhang, Z. Li, H. Li, X. Zhou, X. Liu, Y. Duan, P. H. Lin, P. Duann, X. Xie, J. Ma, Z. Liu and J. Guan, *Biomacromolecules*, 2017, **18**, 2820-2829.
14. Y. Birnbaum, M. C. Fishbein, C. Blanche and R. J. Siegel, *New England Journal of Medicine*, 2002, **347**, 1426-1432.
15. T. D. Johnson and K. L. Christman, *Expert Opin Drug Del*, 2013, **10**, 59-72.
16. S. Suarez, A. Almutairi and K. L. Christman, *Biomater Sci*, 2015, **3**, 564-580.
17. Y. T. Ho, B. Poinard and J. C. Kah, *Nanomedicine (Lond)*, 2016, **11**, 693-714.
18. T. Dvir, M. Bauer, A. Schroeder, J. H. Tsui, D. G. Anderson, R. Langer, R. Liao and D. S. Kohane, *Nano Lett.*, 2011, **11**, 4411-4414.
19. X. Xue, X. Shi, H. Dong, S. You, H. Cao, K. Wang, Y. Wen, D. Shi, B. He and Y. Li, *Nanomedicine*, 2018, **14**, 619-631.
20. R. C. Scott, J. M. Rosano, Z. Ivanov, B. Wang, P. L. Chong, A. C. Issekutz, D. L. Crabbe and M. F. Kiani, *FASEB J*, 2009, **23**, 3361-3367.
21. S. Zhang, J. Li, S. Hu, F. Wu and X. Zhang, *Int J Nanomedicine*, 2018, **13**, 4045-4057.

22. C. X. Zhang, Y. Cheng, D. Z. Liu, M. Liu, H. Cui, B. L. Zhang, Q. B. Mei and S. Y. Zhou, *J Nanobiotechnology*, 2019, **17**, 18.
23. M. P. Monopoli, C. Åberg, A. Salvati and K. A. Dawson, *Nature Nanotechnology*, 2012, **7**, 779.
24. M. M. Nguyen, A. S. Carlini, M. P. Chien, S. Sonnenberg, C. Luo, R. L. Braden, K. G. Osborn, Y. Li, N. C. Gianneschi and K. L. Christman, *Advanced materials*, 2015, **27**, 5547-5552.
25. F. G. Spinale, M. L. Coker, S. R. Krombach, R. Mukherjee, H. Hallak, W. V. Houck, M. J. Clair, S. B. Kribbs, L. L. Johnson, J. T. Peterson and M. R. Zile, *Circ. Res.*, 1999, **85**, 364-376.
26. R. Mukherjee, T. A. Brinsa, K. B. Dowdy, A. A. Scott, J. M. Baskin, A. M. Deschamps, A. S. Lowry, G. P. Escobar, D. G. Lucas, W. M. Yarbrough, M. R. Zile and F. G. Spinale, *Circulation*, 2003, **107**, 618-625.
27. J. T. Peterson, H. Hallak, L. Johnson, H. Li, P. M. O'Brien, D. R. Sliskovic, T. M. A. Bocan, M. L. Coker, T. Etoh and F. G. Spinale, *Circulation*, 2001, **103**, 2303-2309.
28. K. Y. DeLeon-Pennell, C. A. Meschiari, M. Jung and M. L. Lindsey, *Prog Mol Biol Transl Sci*, 2017, **147**, 75-100.

## Chapter 3: Degradable nanoparticles localize and clear from the heart and satellite organs

### 3.1 Introduction

As previously discussed, treatment during the acute phase of MI is limited to minimally invasive therapeutic strategies. With this in mind, we focused our efforts on the development of polynorbornene-based nanoparticle therapeutics that aggregate in response to matrix metalloproteinase cleavage, leading to preferential localization in the infarcted heart. We have proven the success of this targeting mechanism[1] as well as confirmed the ability of this platform to carry and deliver a small molecule MMP-inhibitor as a therapeutic payload.[2]

While our previous nanoparticle demonstrated successful localization and drug-carrying capabilities, it is limited by the fact that is a non-degradable material, meaning that its accumulation in the heart or any off-target tissues was permanent. While this system served as an excellent proof of concept that demonstrated successful infarct-targeting utilizing endogenous MMP-cleavage, we wanted to improve upon this system by engineering a new material that could be broken down and cleared from the body over time while still undergoing a morphological switch to enhance targeting to the heart over conventional targeting methods. While many kinds of degradable polymers have been developed[3-5], very few have demonstrated the ability to functionalize the backbone with biologically relevant moieties. Additionally,

To achieve this, we utilized ring-opening metathesis polymerization (ROMP), a synthesis method that allows for narrow molecular weight distributions and complex structures. Copolymerization of a 1,3-dimethyl-2-phenoxy-1,3,4,7-tetrahydro-1,3,2-diazaphosphepine 2-oxide (MePTDO) and norbornene monomers yielded polymers that underwent degradation into smaller molecular weight fragments through the cleavage of acid-labile phosphoramidate

linkages.[6] This mechanism of degradation is particularly suitable for applications in the heart due to the acidic alteration of pH during the acute phase of MI.[7] Thus, we sought to utilize this degradable polymer with our previously established MMP-responsive peptide sequence for targeting the infarcted myocardium. In this chapter, we will investigate the ability of this degradable nanoparticle to aggregate and clear over time in the infarcted region of the heart and satellite organs.

## 3.2 Results

### *3.2.1 Degradable nanoparticle synthesis and enzyme responsiveness (Done by Yifei Liang)*

To examine whether these degradable nanoparticles can be used as a targeted delivery platform, we first examined its enzyme responsiveness in vitro. A Cy5.5-labeled nanoparticles were formulated at 300 µM with respect to polymer concentration (**Figure 3.1 A-B**). This concentration was selected based on previously established procedures for in vivo intravenous (IV) injection.[1] Upon overnight treatment with thermolysin, which is a more thermostable alternative of MMP, a morphological switch into microscale assemblies was observed via TEM, indicating degradable NPs maintained enzyme responsiveness as their non-degradable polynorbornene analog (**Figure 3.1 C**).

### *3.2.2 Cytocompatibility*

Following treatment of L929s with various physiologically relevant concentrations of degradable nanoparticles ranging from 60 µM to 0.5 µM, we observed no significant decrease in metabolic activity compared to a healthy control. The maximum concentration was chosen set at 3.5 times the initial dilution of 300µM degradable nanoparticles into the blood volume of a 250g female Sprague-Dawley rat (~16 mL)[8], which is roughly ~17 µM.

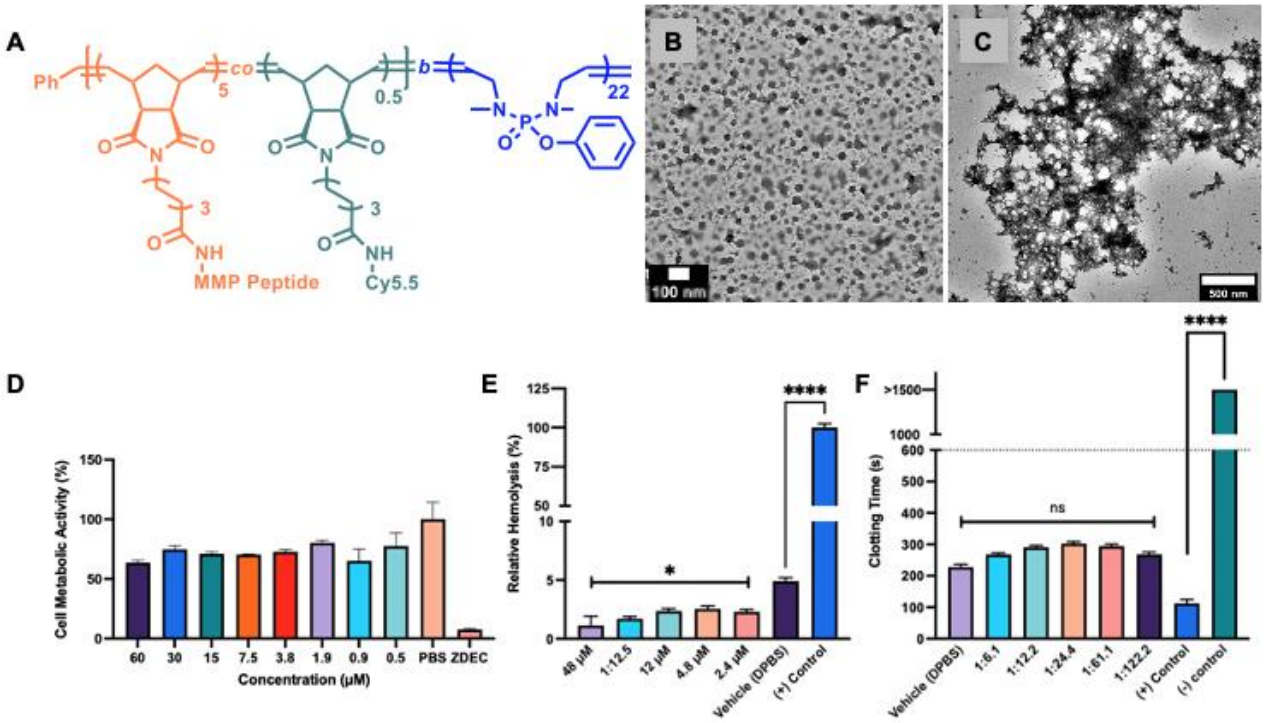


**Figure 3. 1: Enzyme responsiveness, cytocompatibility, and hemocompatibility of Cy5.5 labeled peptide-polyphosphoramidate nanoparticles.**

(A) Chemical structure of peptide brush polyphosphoramidate. TEM images of (B) nanoparticles and (C) aggregates formation post incubation with thermolysin at 1:100 thermolysin:polymer for 24 h a 37 °C in DPBS. Scale bar: 100 nm. (D) Cytocompatibility of NPs with L929 at various concentrations between 0.5 and 60 μM. For reference, the concentration of polymer in blood post IV injection is approximately 17.6 μM. (E) Percent hemolysis of red blood cells post incubation with NPs at various concentrations. Absorbance was measured at 540 nm. (F) Activated clotting times of whole human blood in the presence of NPs at different concentrations. Dotted line at 600 seconds defines the threshold for clotting time response (n = 4) ns ($p > 0.05$), and **** ($p \leq 0.0001$). Values are displayed as mean ± SEM. (Panels B, C, E, and F acquired from Yifei Liang)

*3.2.3 Hemocompatibility (Done by Yifei Liang)*

To assess the hemocompatibility of these NPs, in vitro red blood cell (RBC) hemolysis and whole blood activating clotting time (ACT) assays were performed. In the RBC hemolysis assay, absorbance of isolated RBCs treated with NPs was used to determine hemolytic activity. As compared to the vehicle (DPBS) control, the NPs did not show any significant difference in percent

hemolysis **(Figure 3.1 E)**. In the ACT assay, viscosity of human whole blood treated with NPs over a range of dilutions was assessed by a Hemochron instrument. The NPs performed similarly to the vehicle control (DPBS), though did show minimal anti-coagulative properties. However, the NP treatments all had ACTs well below the range of the negative control and physiologically relevant upper bound (600 seconds) **(Figure 3.1 F)**. These results suggested that the NPs are hemocompatible and suitable for in vivo use.

*3.2.4 Localization*

Following intravenous injection one-day post-MI, we observed strong degradable nanoparticles localization in the infarcted region of the heart. Similar to our non-degradable platform, we also observe regioselective accumulation in the infarcted region with very little retention in the border zone or remote myocardium. Additionally, the morphology of the accumulation resembles a bolus, practically filling the infarcted myocardium with material (**Figure 3.2 A**). In the border zone (**Figure 3.2 B**) and remote myocardium (**Figure 3.2 C**), degradable nanoparticles appear more punctate in morphology.

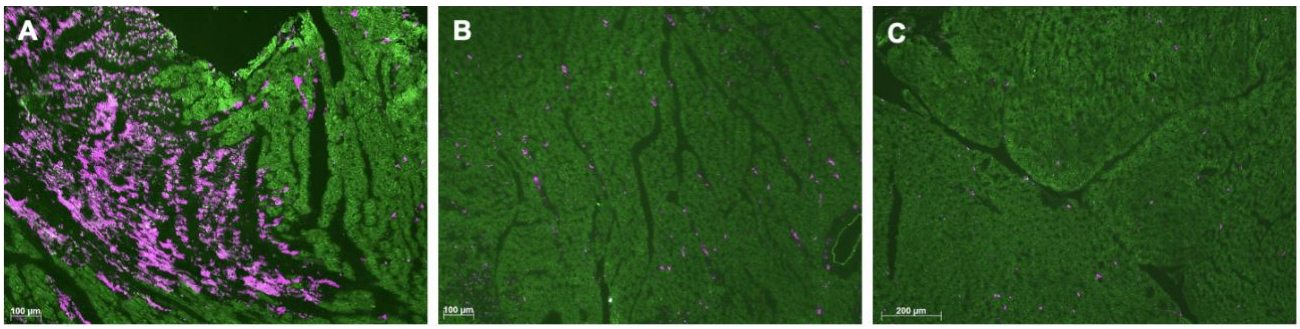


**Figure 3. 2: Regioselective nanoparticle accumulation in the infarcted heart.**
Degradable nanoparticle signal in the infarcted left ventricle (A), borderzone (B), and remote myocardium (C). Scale bar are 100um.

*3.2.5 Biodistribution*

At one day post-injection, degradable nanoparticles display strong accumulation in the heart, liver, and kidneys (**Figure 3.3 A**). Beyond targeting the myocardium, off-target accumulation in the liver and kidneys is typical for intravenously injected nanoparticles[9]. We continued to observe strong signal in the heart and kidneys at 7 days (**Figure 3.3 B**) but, via LiCor scans, noticed a drop off in signal in all the organs at 14 (**Figure 3.3 C**) and 28 days post-injection (**Figure 3.3 D**).

Immunohistochemistry revealed a stark decrease in degradable nanoparticles presence in the infarcted heart from 1 to 7 days post injection (**Figure 3.3 E and F**). At 7 days we observed a change in degradable nanoparticles morphology as well, going from “brushstroke-like” distribution to a more dispersed distribution of punctate aggregated. This type of morphology continued at 14 (**Figure 3.3 G**) and 28 (**Figure 3.3 H)** days post-injection.

As we look at further timepoints, quantification of LiCor scans showed that degradable nanoparticles signal significantly decreases over time in the left ventricle at 7 days post-injection with further reduction in signal at 14 days (**Figure 3.3 I**). This trend is also observed in the satellite organs; of particular interest is the decreased accumulation in the clearance organs, the liver and kidneys (**Figure 3.3 J**).

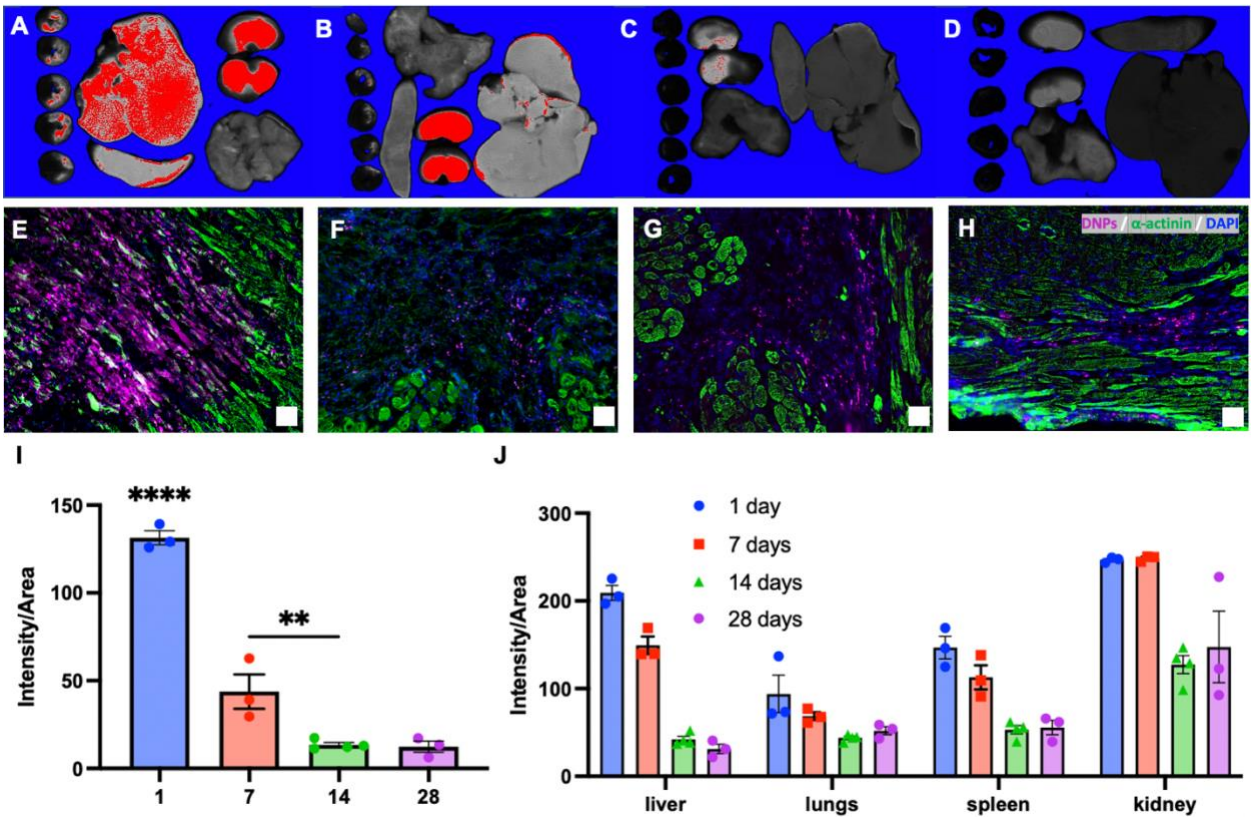


**Figure 3. 3: Degradable nanoparticle biodistribution over time.**
LiCor scans of the heart and satellite organs at 1-day (A), 7 days (B), 14 days (C), and 28 days (D) post-injection of degradable nanoparticles (n = 3 at each timepoint). Quantification of nanoparticle signal in the left ventricle (E) and satellite organs (F) from LiCor organ scans.

When comparing the biodistribution between our original and degradable systems, we observe a significant decrease of degradable nanoparticles signal in the spleen accompanied by a significant increase in accumulation in the kidneys and left ventricle (LV) (**Figure 3.4 A**). Histology corroborated the differences in material accumulation in the infarcted left ventricle, showing stark decrease in material starting at 7 days post-injection. Additionally, with regards to material morphology, the original MMP NP system accumulated in punctate aggregates (**Figure**

**3.4 B**) whereas the degradable system appears to accumulate to a much higher degree along the direction of the cardiomyocytes (**Figure 3.4 C**), filling the infarct with material.

While we did not investigate the biodistribution over time of our previous system, due to its non-degradable nature we assume that all off-target accumulation led to retention out to 28 days and beyond, as was observed in the heart. The decrease in degradable nanoparticles signal over time implies that this degradable system is not only clearing from the heart but also the satellite organs, indicating that it is clearing from the body through bile and/or urine excretion.

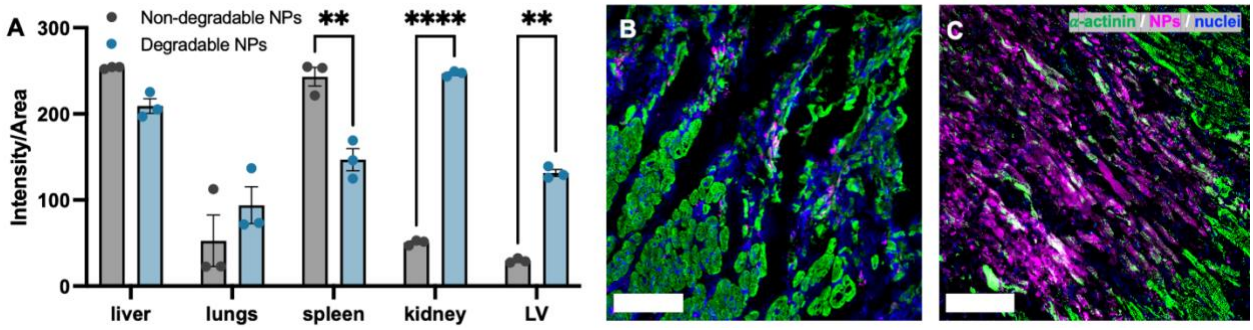


**Figure 3. 4: Degradable nanoparticle biodistribution and accumulation compared to its non-degradable analog.**
(A) Comparison of biodistribution of the original non-degradable platform to the degradable nanoparticles at 1-day post-injection. Immunohistochemistry for cardiomyocytes at one day post-injection for the non-degradable (B) and degradable nanoparticle (C) platforms. Scale bars are 50μm. **($p \leq 0.01$), **** ($p \leq 0.0001$) via Two-Way ANOVA with Šidák's correction. Values are displayed as mean ± SEM.

*3.2.6 Histology*

To better understand how degradable nanoparticles are accumulating and interacting with cardiomyocytes and immune cells in the heart, we used confocal microscopy to generate higher resolution images from stained tissue. We demonstrated that unique degradable nanoparticle morphology at 1-day post-injection was primarily driven by uptake of the material by

cardiomyocytes in the necrotic core of the infarcted heart demonstrated by the colocalization of α-actinin and the cy5.5 labeled- degradable nanoparticles (**Figure 3.5 A**). At 14 and 28 days post-injection we observed macrophage uptake of degradable nanoparticles in the infarcted region of the heart (**Figure 3.5 B and C**).

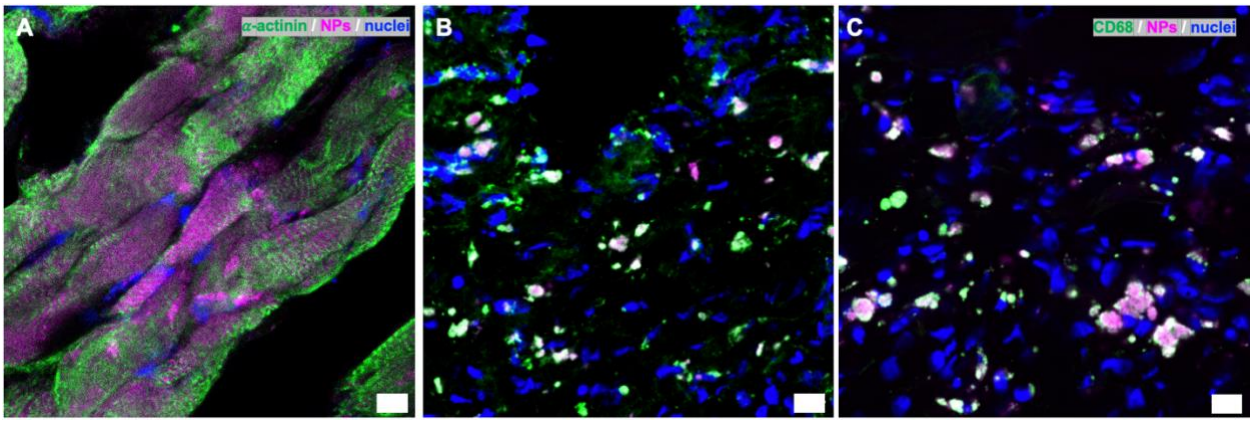


**Figure 3. 5: Degradable NP interaction with cells in the heart over time.**
(A) Degradable nanoparticles localize to cardiomyocytes within in the necrotic core of the infarct. At 14 (B) and 28 days (C) post-injection, degradable nanoparticles demonstrate colocalization with $CD68^{+}$ macrophages in the infarcted myocardium.

### 3.3 Discussion

This degree of degradable nanoparticle accumulation in the infarcted heart is particularly impressive from an intravenous injection and displays enhanced accumulation over the previously non-degradable nanoparticle platform. Beyond the enhanced accumulation in the myocardium, we also observed substantial degradable nanoparticle signal in the kidneys and liver. Interestingly, over time the signal in all organs, including the heart, decreased. This strengthens the hypothesis that degradable nanoparticles are being broken down and cleared *in vivo*.

We hypothesize that the observed decrease in nanoparticle signal from the kidneys and liver is due to the degradable nature of the polymer backbone. Post-formulation, the polymer

backbone has a comparable degree of polymerization to its non-degradable counterpart, however, as the material begins to be broken down via hydrolysis at acidic conditions, those polymer fragments have a low enough molecular weight to be cleared from the body through bile and urine. By 28 days there is very little degradable nanoparticle signal in the heart and satellite organs, allowing us to infer that a bulk of the initially injected material has been cleared from the body, although further studies of bodily excretions (urine, fecal matter) and examination of degradable nanoparticle biodistribution at longer timepoints would need to be performed confirm this.

When comparing the biodistributions of this degradable system to our previous non-degradable platform, we observed significantly higher accumulation in the infarcted left ventricle and kidneys. We hypothesize that as the degradable nanoparticle is broken down into smaller molecular weight fragments via hydrolysis of acid-labile linkages in the polymer backbone, this allows for cellular uptake in the heart that was not previously observed. Because we observed nanoparticle uptake as soon as 1 day post-injection, the degradation process could begin as soon as the material enters the acidic environment of the heart, inciting hydrolysis of the polymer backbone. Additionally, as previously mentioned, these lower molecular weight fragments are more amenable to passage through the kidney's glomerular filtration barrier, which requires a minimum diameter of less than 6 nanometers for guaranteed diffusion through the glomerular basement membrane.[10]

As we began to better understand the retention and biodistribution of degradable nanoparticles over time, we also wanted to understand what kinds of cells were interacting with these nanoparticles. Staining for cardiomyocytes revealed colocalization of alpha-actinin (cardiomyocytes) and cy5.5-labeled degradable nanoparticles. As cardiomyocytes begin to

display a necrotic phenotype and their cell membranes become compromised[11], fragments of partially degraded degradable nanoparticles are uptaken into the cell body. To our knowledge, this kind of cellular uptake has not been observed from another nanomaterial platform.

We hypothesize that a main mechanism of degradable nanoparticle clearance is through the removal of necrotic cardiomyocytes by macrophages during the acute inflammatory phase.[11] To further investigate this, we performed immunohistochemistry to stain for $CD68^+$ macrophages at 14-, and 28-days post-injection (n = 3 at each timepoint) and observed strong colocalization of degradable nanoparticles with $CD68^+$ macrophages in the infarcted region. It has been previously established that macrophages are able to phagocytose particles up to 5 μm[12], which the remaining degradable nanoparticle aggregates fall under. Thus, we can conclude that at later timepoints post-injection, macrophages are phagocytosing and clearing out the remaining degradable nanoparticles in the extracellular matrix. Knowing that degradable nanoparticles are initially localized to necrotic cardiomyocytes and then macrophages in the heart will allow us to make an informed decision about what sort of therapeutic payload to deliver using this platform.

In this chapter, we explored the feasibility of administering a degradable nanoparticle to the heart following acute myocardial infarction. We established this platform's ability to strongly localize to the heart and be uptaken by cardiomyocytes and macrophages, depending on the timepoint post-injection. The development of a degradable polymeric nanoparticle system that demonstrates true clearance not only in the target tissue but also in clearance organs has higher potential for clinical translation in applications beyond acute myocardial infarction. Future studies will investigate the therapeutic efficacy of this degradable platform in a model of acute myocardial infarction once a therapeutic is conjugated to the polymer backbone.

### 3.4 Methods

*Nanoparticle Cytocompatibility*

For cytocompatibility assessment, murine fibroblast cells (L929) were used in accordance with the UNI ISO 10993/2009 for cytotoxicity assays. Cells were plated and left to adhere overnight. Following cell adhesion, degradable nanoparticles were added at physiologically relevant concentrations spanning 60-0.5μM with PBS and zinc diethyldithiocarbamate (ZDEC) serving as positive and negative controls, respectively. Treated cells were then incubated for 24 hours before performing an Alamar Blue assay to evaluate their metabolic activity. All treatments were normalized to the healthy PBS control.

*Nanoparticle Dilutions for Hemocompatibility (Performed by Yifei Liang)*

According to previously optimized surgical procedures, 1 mL nanoparticle solution at 300 μM regarding polymer can be injected intravenously into rat with myocardial infarction. Under the assumption that a 250 g rat has 16 mL of blood, polymer concentration in bloodstream is approximately 17.6 μM. Therefore, nanoparticle stock solutions at 600, 300, 150, 60 and 30 μM in 1X DPBS without $Ca^{2+}$ and $Mg^{2+}$ were prepared using serial dilutions.

*Activated Clotting Time (ACT) Assay with Whole Human Blood (Performed by Yifei Liang)*

Stocks of NPs were added to whole human blood so that final polymer concentrations were 49.0, 24.5, 12.2, 4.91, 2.45 μM. 1X DPBS without $Ca^{2+}$ and $Mg^{2+}$ was used as the vehicle control, ground glass as the positive control, and no $Ca^{2+}$ as the negative control treatment. Using a calibrated Hemochron 801 instrument, activated clotting time of the NPs in recalified citrated human whole blood was assessed. Briefly, Hemochron P214 tubes with glass beads were warmed and 4 μL of $CaCl_2$ (2.2 M) and 36 μL of NP stock or control additive was added to each tube, gently mixed, and allowed to incubate for 30 s at 37 °C (n=4). Citrated human whole blood

(400 µL) was added to each tube (t=0), mixed by hand for 10-15 seconds, and inserted into the instrument. Clot formation was determined by the displacement of the magnet within the tube. The time to clot formation was recorded for each sample. The negative controls (blood samples without calcium) exceeded the maximum time range of the instrument (>1500 s). The ACTs for the NPs are reported in comparison to the positive and negative controls.

*Hemolysis of Red Blood Cells (RBCs) (Performed by Yifei Liang)*

Stocks of NPs were added to the isolated red blood cells (RBC) so that final polymer concentrations were 48, 24, 12, 4.8, 2.4 µM. 1X DPBS without $Ca^{2+}$ and $Mg^{2+}$ was used as the vehicle control and 1% Triton X-100 as the positive control treatment. RBCs were isolated from 40 mL of citrated human whole blood via centrifugation at 500 x g for 5 min. Supernatant was removed and replaced with 150 mM NaCl solution. The RBCs were gently mixed and re-isolated with centrifugation. Gentle washes with DPBS were repeated three times. Once isolated, the RBCs were diluted 1:50 in 1X DPBS and gently mixed. RBCs (184 µL) were treated with NP dilutions (16 µL) in a clear 96-well plate and incubated for 1-hour at 37 °C (n=6). Due to the innate color of the dye-labeled NPs, 16 µL of NP dilutions was incubated with 184 µL of DPBS in parallel to adjust absorbance values (n=3). Plates were centrifuged at 500 x g for 10 min to form a pellet of intact RBCs. 100 µL of the supernatant from each well was carefully transferred to a fresh, clear 96-well plate. Absorbance measurements were taken to determine hemolysis and recorded at 405 nm, 450 nm, and 540 nm as well as representative full spectra from each experimental group. Plate reader measurements were conducted on an EnSpire Multimode Plate Reader. Hemolysis was determined by correcting for the background absorbance of the plate and respective absorbance from each sample group of parallel NPs in DPBS and then normalized to 1% Triton X-100-treated RBCs (representing 100% hemolysis). Hemocompatibility analysis was

performed similarly as described by Carlini et al.[13, 14] Statistical comparisons were performed using a one-way ANOVA.

*Surgical procedures and IV injection*

All procedures in this study were approved by the Committee on Animal Research at the University of California, San Diego and the Association for the Assessment and Accreditation of Laboratory Animal Care. Female, Sprague Dawley rats (225 – 250g) underwent ischemia-reperfusion (IR) procedures via left thoracotomy and temporary occlusion of the left anterior descending artery for 35 minutes[15]. One day post-MI, animals were anesthetized using isoflurane and randomly intravenously injected with 1 mL of NPs (300μM) and harvested at 1, 7, 21, and 28 days post-injection (n = 3 for each timepoint). Animals were euthanized via overdose of pentobarbital (200 mg/kg) and the satellite organs (kidney, spleen, lungs, and liver) were collected for LiCor analysis. The heart was excised and matrix sliced into 5 sections for LiCor analysis and immunohistochemistry.

*LiCor whole organ scanning and quantification*

Organs were kept on ice until scanning. A clear transparency was placed on the scanner and the organs were arranged and scanned at intensity level 1 at the 700-nanometer wavelength with an offset of 1 millimeter. Scanned images were analyzed using a custom MATLAB script where individual organs were outlined and analyzed for Cy5.5 fluorescence intensity per area. Statistical comparisons were performed using a two-way ANOVA.

*Immunohistochemistry (a-actinin, CD68)*

Following euthanasia, hearts sliced into 5 sections and embedded in OCT for cryosectioning. Hearts were sectioned to a thickness of 10 μm sections were stained with anti-α-actinin (1:75

dilution, Sigma) and Alexa Fluor-488 (1:500 dilution, ThermoFisher). To identify macrophages, sections were stained with anti-CD68 (1:100 dilution, BioRad) and Alexa Fluor-488 (1:500 dilution, ThermoFisher). Slides were imaged using a Keyence BZ-X Series all-in-one fluorescent microscope and a Zeiss LSM 780 confocal microscope.

### 3.5 Acknowledgements

The authors would like to acknowledge their funding sources 1R01HL139001, additionally HLS was supported by F31 HL152610-03. We would like to acknowledge the Stem Cell and Genomics core in the Sanford Consortium for Regenerative Medicine for use of their microscopes.

Chapter 3 is currently being prepared for submission for publication of the material, Holly Sullivan, Yifei Liang, Kendra Worthington, Colin Luo, Nathan C. Gianneschi, Karen L. Christman. “Degradable Poly(phosphoramidate): Efficient Synthesis, Peptide Functionalization, and Targeted Delivery to the Infarcted Heart”. The dissertation author will be a co-first author of this paper.

### 3.6 References


1. M. M. Nguyen, A. S. Carlini, M. P. Chien, S. Sonnenberg, C. Luo, R. L. Braden, K. G. Osborn, Y. Li, N. C. Gianneschi and K. L. Christman, *Adv Mater*, 2015, **27**, 5547-5552.
2. H. L. Sullivan, Y. Liang, K. Worthington, C. Luo, N. C. Gianneschi and K. L. Christman, *bioRxiv*, 2022, DOI: 10.1101/2022.03.07.483374, 2022.2003.2007.483374.
3. W. J. Neary and J. G. Kennemur, *Macromolecules*, 2017, **50**, 4935-4941.
4. A. Hejl, O. A. Scherman and R. H. Grubbs, *Macromolecules*, 2005, **38**, 7214-7218.
5. K. Song, K. Kim, D. Hong, J. Kim, C. E. Heo, H. I. Kim and S. H. Hong, *Nature Communications*, 2019, **10**.
6. Y. Liang, H. Sun, W. Cao, M. P. Thompson and N. C. Gianneschi, *ACS Macro Letters*, 2020, **9**, 1417-1422.
7. N. G. Frangogiannis, *Compr Physiol*, 2015, **5**, 1841-1875.
8. H. B. Lee and M. D. Blaufox, *J Nucl Med*, 1985, **26**, 72-76.
9. W. Poon, Y.-N. Zhang, B. Ouyang, B. R. Kingston, J. L. Y. Wu, S. Wilhelm and W. C. W. Chan, *ACS Nano*, 2019, **13**, 5785-5798.
10. J. Liu, M. Yu, C. Zhou and J. Zheng, *Materials Today*, 2013, **16**, 477-486.
11. M. Chiong, Z. V. Wang, Z. Pedrozo, D. J. Cao, R. Troncoso, M. Ibacache, A. Criollo, A. Nemchenko, J. A. Hill and S. Lavandero, *Cell Death & Disease*, 2011, **2**, e244-e244.
12. W. P. Lafuse, D. J. Wozniak and M. V. S. Rajaram, *Cells*, 2020, **10**.
13. J. N. Barbosa and D. P. Vasconcelos, in *Handbook of Biomaterials Biocompatibility*, ed. M. Mozafari, Woodhead Publishing, 2020, DOI: https://doi.org/10.1016/B978-0-08-102967-1.00003-7, pp. 43-52.
14. A. S. Carlini, R. Gaetani, R. L. Braden, C. Luo, K. L. Christman and N. C. Gianneschi, *Nat Commun*, 2019, **10**, 1735.
15. A. S. Carlini, W. Choi, N. C. McCallum and N. C. Gianneschi, *Advanced Functional Materials*, 2021, **31**.
16. J. M. Singelyn, P. Sundaramurthy, T. D. Johnson, P. J. Schup-Magoffin, D. P. Hu, D. M. Faulk, J. Wang, K. M. Mayle, K. Bartels, M. Salvatore, A. M. Kinsey, A. N. Demaria, N. Dib and K. L. Christman, *J Am Coll Cardiol*, 2012, **59**, 751-763.

## Chapter 4: Protein-like polymers as a nanoscale platform for targeting the infarcted heart

### 4.1 Introduction

While nanoparticle platforms have demonstrated their relevance as successful minimally invasive vehicles for administering therapeutics to the injured heart, as discussed in literature and the preceding chapters, there remains several drawbacks to the translation in the clinic. Of most concern is the off-target accumulation of intravenously administered nanoparticle platforms. As nanoparticles traverse through the systemic circulation, much of the injected material will accumulate in the satellite organs such as the liver, spleen, and kidneys. This phenomenon diverts much of the intended therapeutic payload from the site of interest, in our case, the heart.

While we have previously discussed nanoparticle systems that have shown the ability to respond to upregulated MMP activity in the heart during the acute phase of MI, we sought to develop a new kind of material that could circumvent the drawbacks of traditional micellar nanoparticle biodistribution. To achieve this, we took inspiration from our previous platforms, namely, the polynorbornene backbone and MMP-responsive peptide sequence for targeted delivery to regions of inflammation[1-4]. However, we aimed to greatly reduce the size and create a more amorphous structure that would be more suitable to systemic circulation. With all this in mind, we engineered a protein-like polymer (PLP), a sub-nano, low molecular weight material that does not assemble into a multi-polymer strand structure and instead acts as a single chain.

Previously, the Gianneschi lab has demonstrated these PLPs resist proteolytic degradation[5], effectively increasing their circulation time, and can be uptaken by cells after responding to stimuli, such as MMP-cleavage *in vitro*.[6] Because of this, we became interested in administering this material in a model of acute myocardial infarction. With these differences in

mind, we hypothesized that PLPs would demonstrate enhanced accumulation in the heart while minimizing off target accumulation due to its protein-like morphology and low molecular weight.

In these studies, we establish the PLP as a promising platform for targeted delivery to the infarcted region of the heart. We also explore the mechanism of accumulation and evaluate material retention in the heart and satellite organs over time.

## 4.2 Results

### *4.2.1 In vitro characterization and cytocompatibility*

PLPs were synthesized via ROMP by Spencer Burton at Northwestern University. The structure of the PLPs is reminiscent of previously discussed materials in that the polynorbornene backbone contains a hydrophobic model therapeutic followed by a cy5.5 fluorescent dye and finally the MMP-responsive peptide sequence (**Figure 4.1 A**). To confirm that PLPs aggregate in response to enzymatic cleavage, they were incubated with thermolysin overnight and then imaged via TEM where micron-scale aggregates had indeed formed following enzymatic cleavage (**Figure 4.1 B**, data collected by Spencer Burton at Northwestern University).

To assess the cytocompatibility of this material, L929s with various physiologically relevant concentrations ranging from 60-0.5μM of PLPs, we observed no significant decrease in metabolic activity compared to a healthy control (**Figure 4.1 C**). Here, the maximum concentration was chosen to be higher than that the initial dilution of PLPs into the blood volume of a rat[7], in this case, ~17μM.

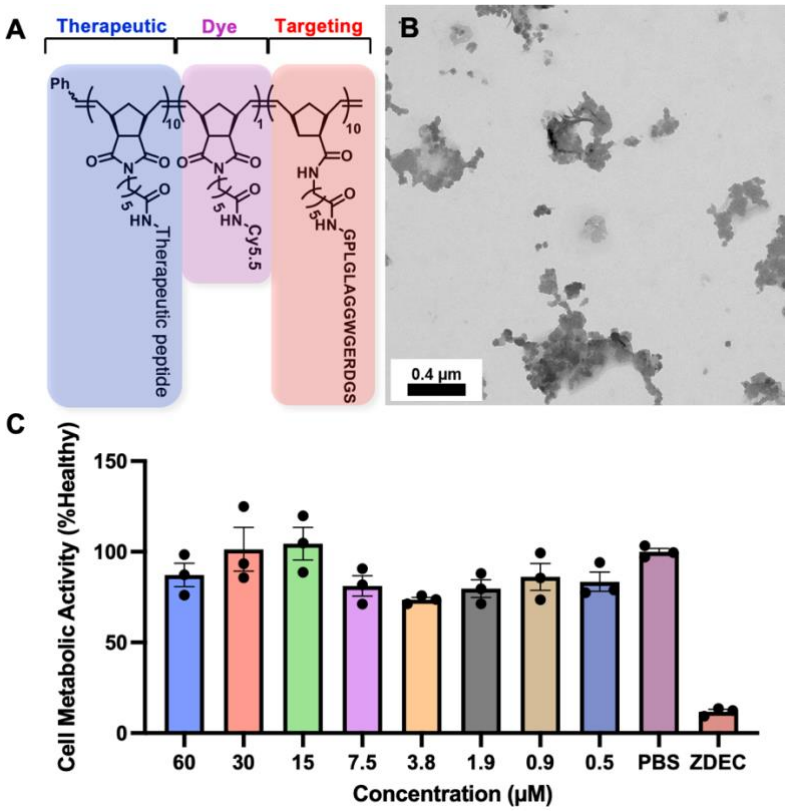


**Figure 4. 1: PLPs are enzyme responsive and cytocompatible.**
(A) PLP structure with three distrinct blocks: therapeutic, dye, and MMP-targeting. (B) TEM image of aggregated PLPs following thermolysin treatment. (C) Cytocompatibility assessment of PLPs at various physiologically relevant concentrations when incubated with L929s. (Image in panel B acquired from Spencer Burton at Northwestern University.)

### *4.2.2 PLP Localization*

Using a rat model of myocardial infarction, we administered the PLPs intravenous via the tail vein at one day post-infarction to evaluate whether the material would target the heart. At one day post-injection, we observed strong PLP localization in the infarcted region of the heart. Similar to our previously mentioned nanoparticle platforms, the PLPs exhibited the most accumulation in the infarct with little material retention in the remote myocardium and borderzone. The morphology of PLPs resembled a bolus style injection with strong signal and spread throughout the entire infarct (**Figure 4.2 A**). There was minimal material localized to the borderzone (**Figure 4.2 B**) and

remote myocardium (**Figure 4.2 C**), and what was observed had more rounded, punctate morphology.

Higher resolution imaging demonstrates that PLPs specifically localized to the infarcted region of the left ventricle (**Figure 4.2 D**) and appear to colocalize with cardiomyocytes within the necrotic core of the infarct (**Figure 4.2 E**). Additionally, visualization of the vasculature in the heart demonstrates that PLPs are able to successfully extravasate from larger vessels within the heart (**Figure 4.2 F and G**).

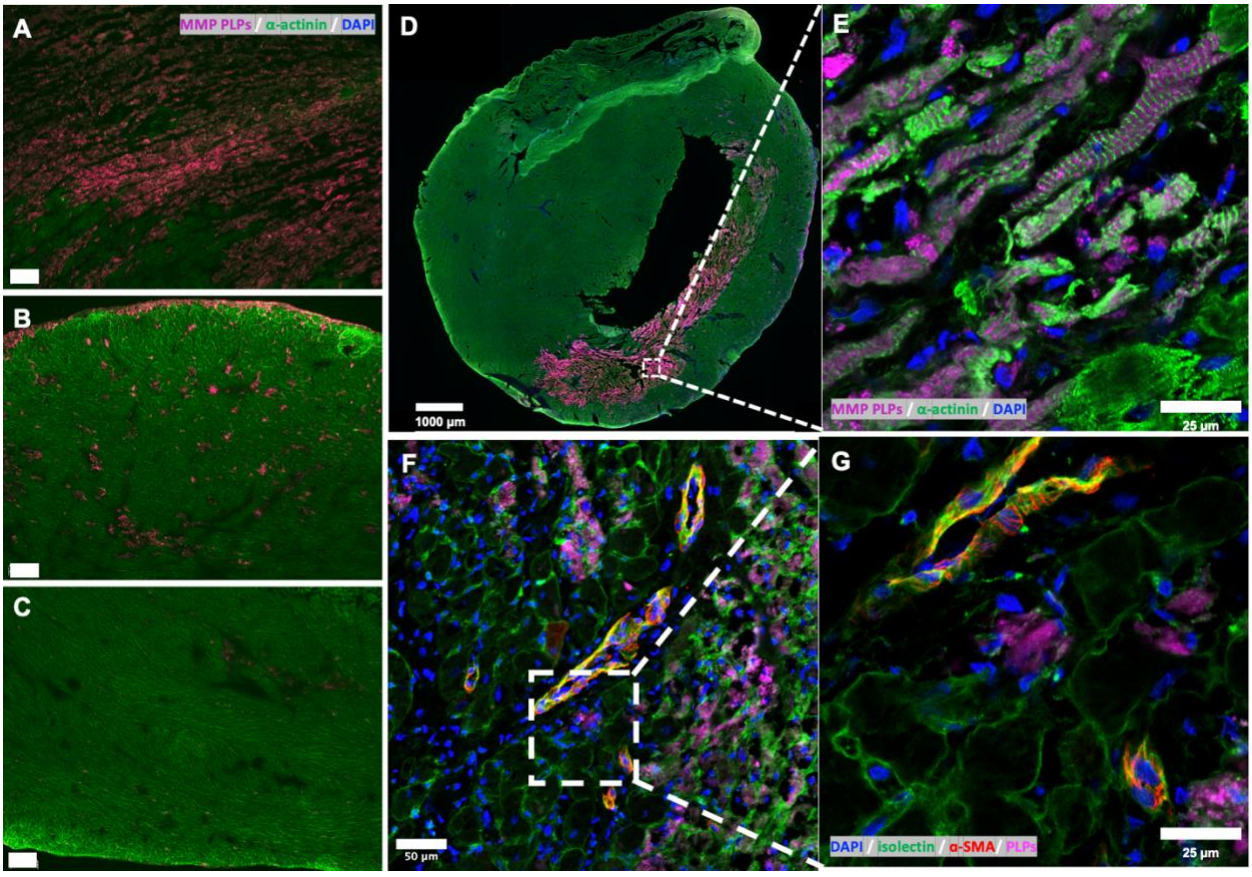


**Figure 4. 2: PLP localization and extravasation in a model of acute MI.**
Cy5.5-labeled PLPs (pictured above in magenta) demonstrate strong localization to the infarcted region of the heart (A) with little accumulation in the remote myocardium (B) with some smaller pockets of aggregates in the borderzone (C). (D) A whole heart slice scan of PLPs in a

heart sacrificed one day post injection at 4x (D) and 63x (E). Vessel staining of tissue at one day post injection at 40x (F) and 63x (G).

### *4.2.3 Biodistribution and cellular uptake in vivo*

PLP biodistribution at one day post-injection was concentrated in the kidneys and infarcted region of the heart (**Figure 4.3 A**); this trend continues at one- and two-weeks post-injection with some increased signal in the liver as well (**Figure 4.3 B and C**). At 4 weeks post-injection, we observed a decrease in signal in the left ventricle but no change in PLP signal in the kidneys (**Figure 4.3 D**). Quantification of LiCor scans showed that though PLP signal shows a trending decrease over time in the left ventricle (Figure 4.3 E), there is no significant difference in this signal over time. Looking at the satellite organs, we confirmed the preferential retention of PLPs in the kidneys over the liver and spleen at all timepoints (**Figure 4.3 F**). Additionally, we observed a decrease in signal in the liver, lungs, and spleen over time, but not the kidneys.

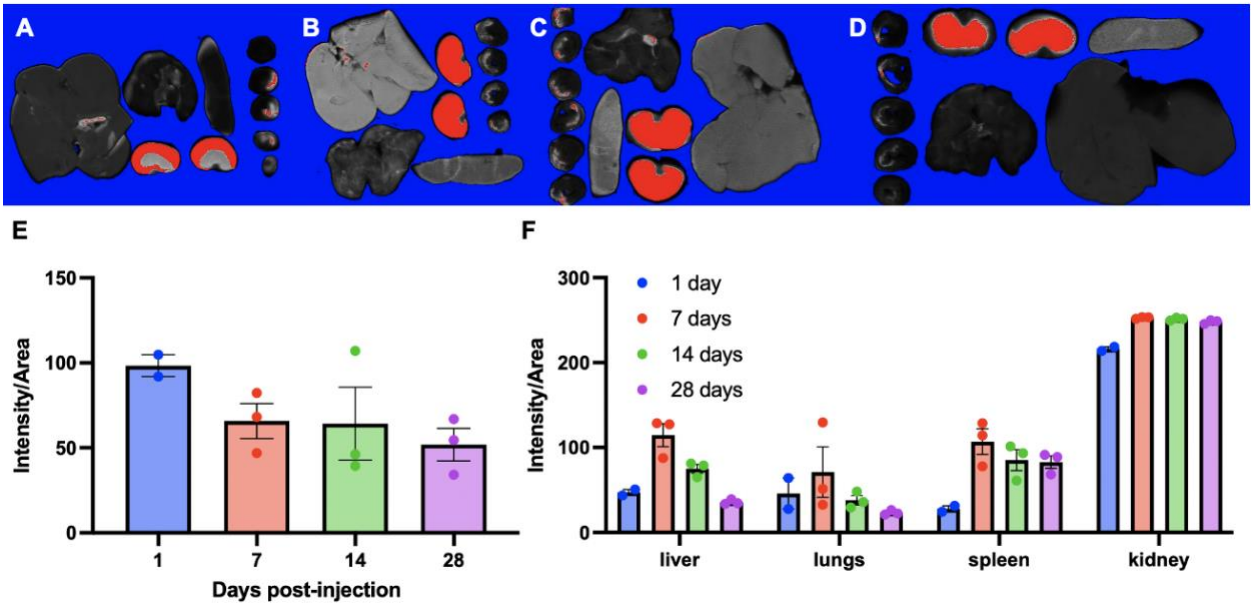


**Figure 4. 3: PLP retention in the heart and satellite organs decreases over time.**
PLP signal in the heart and satellite organs at 1 day (A), 7 days (B), 14 days (C), and 28 days (D) post-injection. Quantification of cy5.5-labeled PLP signal in the left ventricle (E) and satellite organs (F) over time.

When comparing this platform to the previously established MMP-responsive nanoparticles[1], we noticed stark differences in biodistribution. Generally, PLPs demonstrate a higher degree accumulation in the kidneys and infarct (**Figure 4.4 A**) whereas the nanoparticles accumulated more in satellite organs, such as the spleen and liver (**Figure 4.4 B**), as previously discussed. These visual differences were confirmed via quantification of the organ scans (**Figure 4.4 C**).

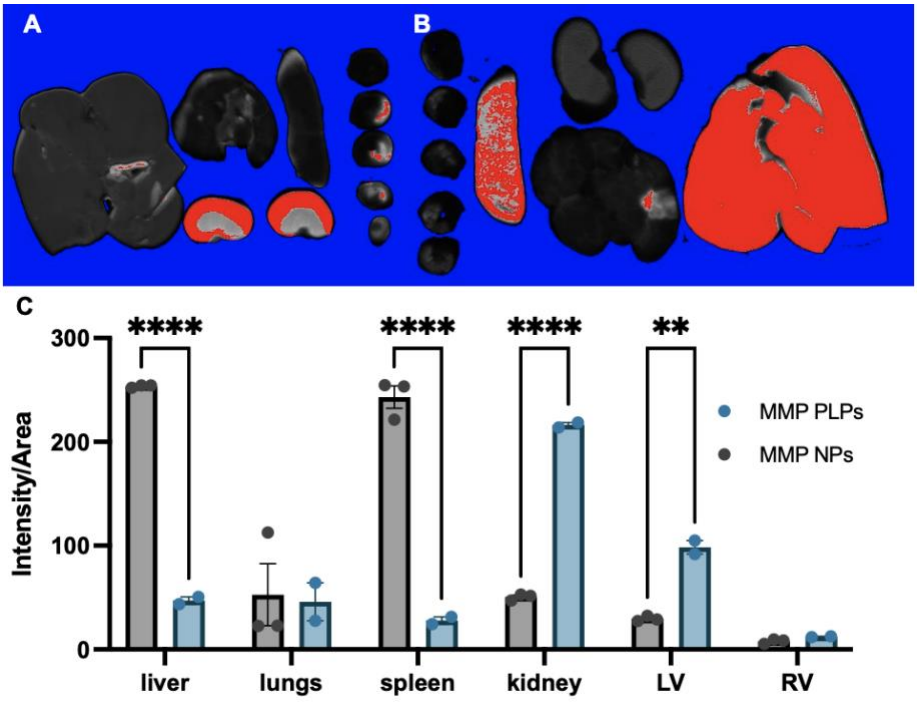


**Figure 4. 4: Comparison of PLP biodistribution to MMP-nanoparticles.**
LiCor organ scans of PLP (A) and MMP-nanoparticles (B) at one day post-injection. (C) MatLab quantification of scans from both platforms demonstrated significant differences in biodistribution between the two platforms, namely in the liver, spleen, kidneys, and LV.

Via histology, we observe a marked decrease in PLP accumulation in the LV from 1 day to 1-week post-injection (**Figure 4.5 A and B**). While the material once completely filled the infarct, at 1 week we observe small, rounded aggregates throughout the injured myocardium. The PLPs maintain this morphology at 2- and 4-weeks post-MI.

Further imaging of $\alpha$-actinin-stained slides revealed strong colocalization of PLPs by cardiomyocytes in the infarcted region of the heart. Via confocal microscopy, we were able to observe what appeared to be cardiomyocyte uptake of PLPs as evidenced by material dispersal amongst the striations of the muscle. At 1 week post-injection, we observed colocalization of PLPs with $CD68^{+}$ macrophages in the infarcted region of the heart (**Figure 4.5 C**).

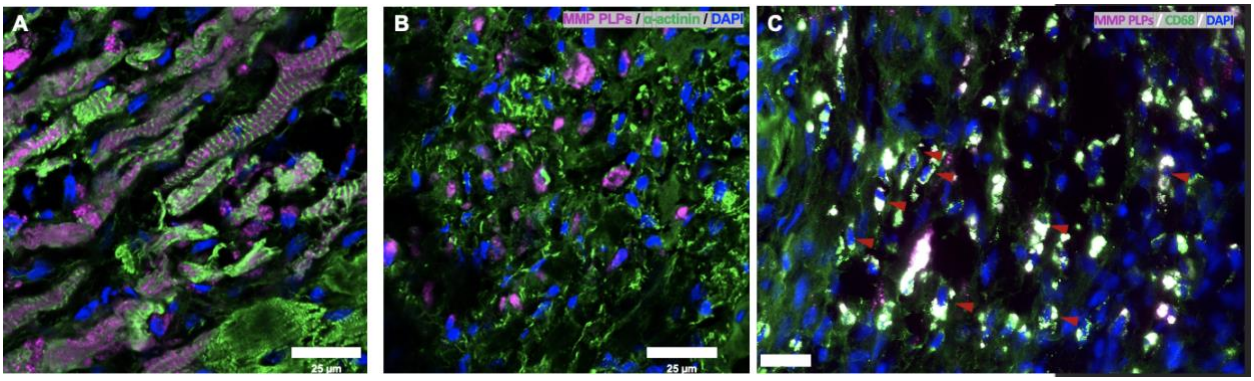


**Figure 4. 5: PLPs are uptaken by cardiomyocytes and CD68+ macrophages in the heart.** PLPs in the infarcted region of the heart and 1 day (1) and 7 days (B) post-injection with α-actinin staining cardiomyocytes. (C) PLPs localize with $CD68^+$ macrophages in the heart at 7 days post-injection, scale bar is 25 µm.

*4.2.4 PLPs are uptaken by necrotic cells*

To confirm that necrotic cells were capable of PLP uptake, we first experimented *in vitro*. After treatment of murine fibroblasts (L929s) with $H_2O_2$ to induce inflammation similar to the infarct environment, PLPs were added followed by staining of live and necrotic nuclei to observe potential cellular uptake of the material. We observed strong colocalization of PLPs by cells that stained positively for calcein (**Figure 4.6 A**) and propidium iodide (**Figure 4.6 B**) to stain live and necrotic nuclei respectively. With this experiment, we expected to see colocalization of the PLPs and both fluorescent stains, indicating cellular uptake of the material by necrotic, dying cells. Looking just at the Cy5.5 channel, representing fluorescently tagged PLPs, we noticed that the material appears to be filling in the cell body, indicating material uptake (**Figure 4.6 C**). Colocalization of PLPs and necrotic cells was confirmed by looking at the merged image where all channels appeared to overlap (**Figure 4.6 D**).

Going a step further, we also administered a co-injection of PLPs and propidium iodide *in vivo* one day post-MI, as it has been previously demonstrated that an intravenous infusion of

propidium iodide labels necrotic nuclei.[8] Fluorescent microscopy of sectioned heart tissue revealed strong colocalization of propidium iodide positive nuclei with Cy5.5-labeled material in the infarcted region of the heart (**Figure 4.6 E and F**).

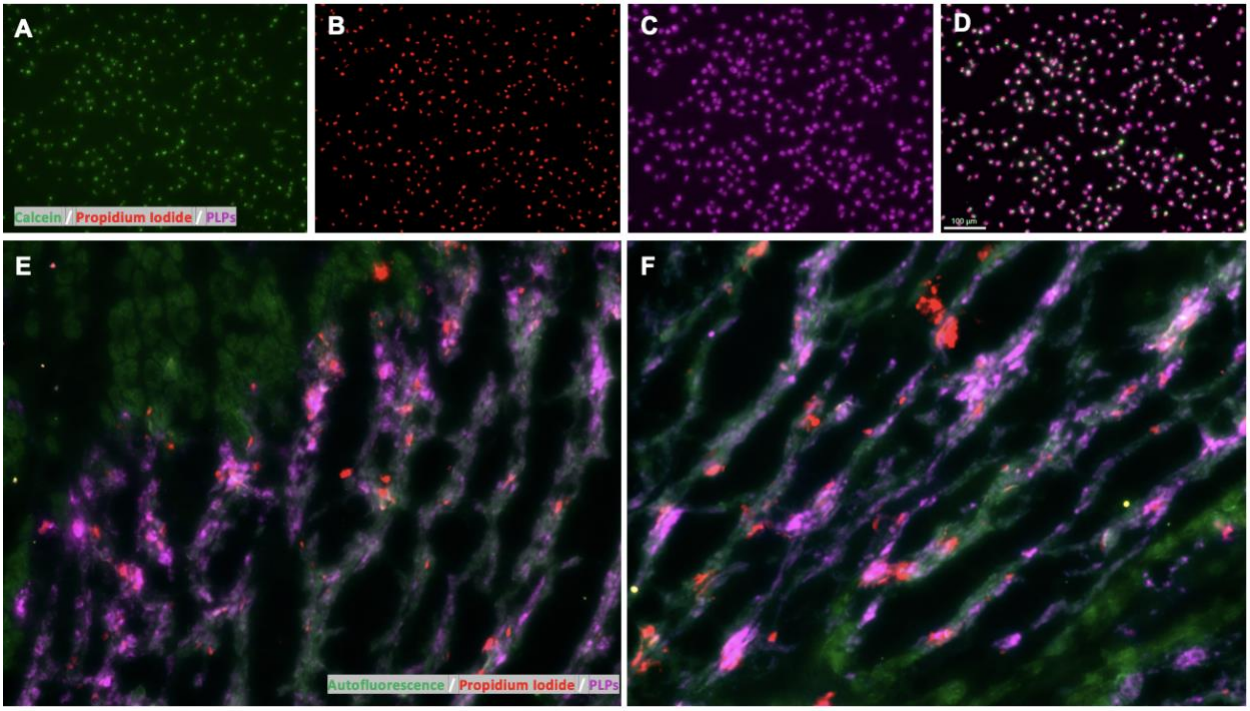


**Figure 4. 6: PLPs are uptaken by necrotic cells in vitro and in vivo.**
Individual channels for calcein (A), propidium iodide (B), and cy5.5-labeled nanoparticles. (C) Merged image demonstrating colocalization of all three channels (calcein, propidium iodide, and Cy5.5), indicating PLP uptake by necrotic, dying cells. (E and F) Colocalization of Cy5.5 and propidium iodide$^{+}$ nuclei in the infarcted region of the heart one day post-injection validated this finding *in vivo*.

*4.2.5. MMP PLP control materials*

Various controls were run to better understand the mechanisms by which PLPs accumulated in the heart and displayed favorable biodistribution in satellite organs. Comparing all control groups

to the biodistribution of the original PLP material (**Figure 4.7 A**), we first injected healthy animals with PLPs and observed no signal in the heart slices and greater material retention in the satellite organs (liver, spleen, and kidneys) (**Figure 4.7 B**). We observed a similar trend in biodistribution with a non-responsive control, a slightly more water-soluble material where we removed the MMP-responsive sequence of the cleavable peptide and instead inserted a glycine-serine spacer (**Figure 4.7 C**). Administration of the therapeutic block only, a less water-soluble material without the MMP-responsive block resulted in high PLP accumulation in all the satellite organs in addition to the infarcted heart (**Figure 4.7 D**). Quantification of all these groups further demonstrated the difference in how altering the PLP drastically affects the biodistribution, specifically in the kidneys, liver, spleen, and heart (**Figure 4.7 E**).

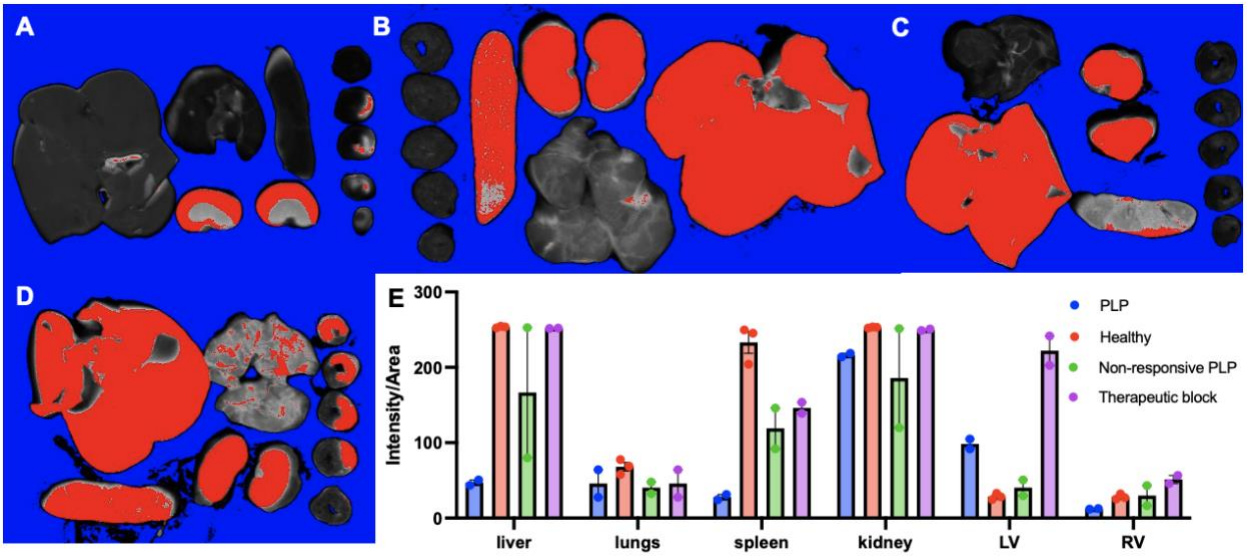


**Figure 4. 7: Control materials demonstrate the importance of MMP-responsiveness and water solubility**
Biodistribution of the original PLP in a model of MI (A), and a healthy animal (B). Injection of two different control materials in a model of MI: a non-responsive PLP (C) and therapeutic block-only (D). All animals were harvested at one day post injection. (D) Quantification of material signal from LiCor scans of the heart and satellite organs.

### 4.3 Discussion

After establishing cytocompatibility at high and physiologically relevant concentrations, we investigated the ability of our PLPs to localize to the infarcted region of the heart *in vivo*. One day post-injection, we observed a significant degree of material accumulation contained within the injured myocardium. We hypothesized that PLPs were being uptaken by cardiomyocytes within the heart after performing confocal imaging of heart tissue slices harvested one day post-injection. More specifically, we hypothesize that the as the necrotic wave begins to sweep through the heart from IR injury, inducing cell swelling and loss of lipid membrane integrity[9], PLPs that have extravasated into the infarcted region are being taken up into resident cardiomyocytes.

To our knowledge, there is no other intravenously administered material that demonstrates this type of uptake in the infarcted heart. Making a direct comparison between the PLPs and our previously published MMP-responsive nanoparticles can help us better understand the characteristics that enable this kind of accumulation. First, and perhaps most importantly, is the difference in molecular weight and morphology between the two platforms. The nanoparticles are composed of many polymers that form the micellar structure, amounting to a diameter of ~100 nm. The PLPs, on the other hand, have a molecular weight of ~31kDa and do not form micelles, instead remain amorphous in structure and ~2-3 nanometers in size, hence the “protein-like” moniker.

We hypothesize that the lower molecular weight and smaller size of the PLP allows it to preferentially accumulate in the kidneys over the liver, where passage through the glomerular basement membrane requires a hydrodynamic radius of less than 6 nm.[10] Additionally, morphology also plays a role in clearance and accumulation. Because of their amorphous, protein-like structure, PLPs have a longer half-life in circulation[5] and a higher aspect ratio,

allowing for easier diffusion through the glomerular filtration barrier.[10] Longer circulation times may also contribute to the significantly higher degree of accumulation we observe in the heart when comparing it to the previously MMP nanoparticle platform. Additionally, we hypothesize that PLP retention in the kidneys will allow for excretion through urine, a clearance pathway which accounts for a majority of drug excretion and is much simpler than hepatic clearance[11]. This is further confirmed by the fact that the filtration-size threshold for globular proteins is < 5 nm in diameter[12].

Next, we demonstrated this material's ability to penetrate into necrotic cells *in vitro* and *in vivo* through propidium iodide-labeling of nuclei. We hypothesize this can also be attributed to its low molecular weight and water solubility. With our control materials we were able to determine the effects of removing or altering certain portions of the PLP. Injection of the therapeutic only represented a purely hydrophobic material and though it made it to the infarcted region, it demonstrated high off target delivery in all the satellite organs. We hypothesize that this material was prematurely aggregating in solution due to the lack of hydrophilic region that the MMP-responsive peptide imparts. This is further exemplified by the non-therapeutic control, where part of the hydrophobic sequence was replaced with a hydrophilic glycine/serine spacer. In this control group we did not observe the same degree of retention in the heart and additionally saw an enhanced degree of signal in the liver. From this we conclude that a balance in the PLP's water solubility is crucial to favorable cardiac accumulation and biodistribution *in vivo.*

In summary, we developed, characterized, and assessed the feasibility of delivering a PLP to the heart during the acute phase of myocardial infarction. We have shown that this new type of polymeric material remains amorphous in morphology, much like a circulating protein, while still aggregating in response to enzymatic cleavage. Compared to our previous nanoparticle

platforms, the PLPs demonstrate a significant increase in accumulation in the heart as well as favorable biodistribution that is biased towards retention in and likely clearance from the kidneys. In addition to increased material retention, we also observed cellular uptake *in vitro* and *in vivo* by necrotic cardiomyocytes. Future studies will assess the therapeutic capabilities of this material on cardiac function and infarct scar size.

### 4.4 Methods

*PLP aggregation assay and TEM*

PLPs (100 μM, with respect to polymer) were treated with thermolysin, an MMP alternative with improved thermostability, (1 μM) or DPBS for 24 hours at 37 °C in 1X DPBS. The resulting nanoparticle solutions were analyzed by dynamic light scattering (DLS) and transmission electron microscopy (TEM) to examine the change in morphology. For the TEM samples, 5 μL of sample was applied to a 400-mesh carbon grid (Ted Pella, Inc.) that had been glow discharged for 15 seconds. 5 μL of 2 wt.% uranyl acetate solution was then applied and wicked away post 30 sec for staining.

*PLP Cytocompatibility*

For cytocompatibility assessment, murine fibroblast cells (L929) were used in accordance with the UNI ISO 10993/2009 for cytotoxicity assays. Cells were plated and left to adhere overnight. Following cell adhesion, PLPs were added at physiologically relevant concentrations spanning 60-0.5μM with PBS and zinc diethyldithiocarbamate (ZDEC) serving as positive and negative controls, respectively. Treated cells were then incubated for 24 hours before performing an Alamar Blue assay to evaluate their metabolic activity. All treatments were normalized to the healthy PBS control.

*Surgical procedures and IV injection*

All procedures in this study were approved by the Committee on Animal Research at the University of California, San Diego and the Association for the Assessment and Accreditation of Laboratory Animal Care. Female, Sprague Dawley rats (225 – 250g) underwent ischemia-reperfusion (IR) procedures via left thoracotomy and temporary occlusion of the left anterior descending artery for 35 minutes[13]. One day post-MI, animals were anesthetized using isoflurane and randomly intravenously injected with 1 mL of PLPs (300μM with respect to polymer) and harvested at 1, 7, 21, and 28 days post-injection (n = 3 for each timepoint). Animals were euthanized via overdose of pentobarbital (200 mg/kg) and the satellite organs (kidney, spleen, lungs, and liver) were collected for LiCor analysis. The heart was excised and matrix sliced into 5 sections for LiCor analysis and immunohistochemistry. This process was repeated for all control materials as well but animals were only harvested at the 1 day post-injection timepoint.

*Propidium Iodide experiments*

To assess the ability of PLPs to be uptaken by necrotic cells *in vitro*, neonatal cardiomyocytes were treated with 500μM $H_2O_2$ for 3 hours to induce inflammation that mimics the infarct environment[14]. Cells were then treated overnight with 50μL of PLPs amounting to a final well concentration of 17μM. After 24 hours of PLP incubation, cells were stained with propidium iodide (Invitrogen) and calcein am (Thermo Fisher) to identify necrotic and live cells, respectively, and imaged on a Keyence BZ-X microscope.

To determine PLP localization to necrotic cells *in vivo*, propidium iodide was resuspended in PBS at 100 mg/mL. That solution was then used to resuspend PLPs at 300μM and sterile filtered for injection. As before, animals who had undergone IR injury one day prior then received a 1 mL of PI + PLPs and were harvested 24 hours post-injection. Hearts were excised and frozen in OCT for cryosectioning.

*LiCor whole organ scanning and quantification*

Organs were kept on ice until scanning. A clear transparency was placed on the scanner and the organs were arranged and scanned at intensity level 1 at the 700-nanometer wavelength with an offset of 1 millimeter. Scanned images were analyzed using a custom MATLAB script where individual organs were outlined and analyzed for Cy5.5 fluorescence intensity per area.

*Immunohistochemistry (a-actinin, CD68)*

Following euthanasia, hearts sliced into 5 sections and embedded in OCT for cryosectioning. Hearts were sectioned to a thickness of 10 μm sections were stained with anti-α-actinin (1:75 dilution, Sigma) and Alexa Fluor-488 (1:500 dilution, ThermoFisher) to visualize cardiomyocytes. Vessels and capillaries were visualized by staining with anti-α-SMA (1:75 dilution, Dako) and Alexa Fluor-647 (1:500 dilution, ThermoFisher) and isolectin (1:75 dilution, Vector Laboratories). To identify macrophages, sections were stained with anti-CD68 (1:100 dilution, BioRad) and Alexa Fluor-488 (1:500 dilution, ThermoFisher). Slides were imaged using a Keyence BZ-X Series all-in-one fluorescent microscope and a Zeiss LSM 780 confocal microscope.

**4.5 Acknowledgements**

I would like to acknowledge my funding sources 1R01HL139001 and F31 HL152610-03. Additionally, I would like to thank our collaborators at Northwestern University: Nathan Gianneschi and Spencer Burton, for synthesizing the material for these experiments. I would like to acknowledge the Stem Cell and Genomics core in the Sanford Consortium for Regenerative Medicine for use of their microscopes.

Chapter 4 is currently being prepared for submission for publication of the material, Holly Sullivan, Spencer Burton, Kendra Worthington, Colin Luo, Nathan C. Gianneschi, Karen L.

Christman. “Protein-like polymers for targeted delivery to the infarct after acute myocardial infarction”. The dissertation author will be a co-first author of this paper.

## 4.6 References


1. M. M. Nguyen, A. S. Carlini, M. P. Chien, S. Sonnenberg, C. Luo, R. L. Braden, K. G. Osborn, Y. Li, N. C. Gianneschi and K. L. Christman, *Adv Mater*, 2015, **27**, 5547-5552.
2. J. L. Ungerleider, J. K. Kammeyer, R. L. Braden, K. L. Christman and N. C. Gianneschi, *Polym Chem*, 2017, **8**, 5212-5219.
3. H. L. Sullivan, Y. Liang, K. Worthington, C. Luo, N. C. Gianneschi and K. L. Christman, *bioRxiv*, 2022, DOI: 10.1101/2022.03.07.483374, 2022.2003.2007.483374.
4. C. E. Callmann, C. V. Barback, M. P. Thompson, D. J. Hall, R. F. Mattrey and N. C. Gianneschi, *Adv Mater*, 2015, **27**, 4611-4615.
5. C. E. Callmann, M. P. Thompson and N. C. Gianneschi, *Accounts of Chemical Research*, 2020, **53**, 400-413.
6. A. P. Blum, J. Yin, H. H. Lin, B. A. Oliver, J. K. Kammeyer, M. P. Thompson, M. K. Gilson and N. C. Gianneschi, *Chemistry – A European Journal*, 2022, **28**, e202103438.
7. H. B. Lee and M. D. Blaufox, *J Nucl Med*, 1985, **26**, 72-76.
8. I. Unal Cevik and T. Dalkara, *Cell Death & Differentiation*, 2003, **10**, 928-929.
9. N. G. Frangogiannis, *Compr Physiol*, 2015, **5**, 1841-1875.
10. J. Liu, M. Yu, C. Zhou and J. Zheng, *Materials Today*, 2013, **16**, 477-486.
11. X. Gu, X. Hao, X. Shen, H. Wang, Y. Zhang and X. Gao, in *Brain Targeted Drug Delivery System*, eds. H. Gao and X. Gao, Academic Press, 2019, DOI: https://doi.org/10.1016/B978-0-12-814001-7.00017-2, pp. 439-454.
12. M. Longmire, P. L. Choyke and H. Kobayashi, *Nanomedicine (London, England)*, 2008, **3**, 703-717.
13. J. M. Singelyn, P. Sundaramurthy, T. D. Johnson, P. J. Schup-Magoffin, D. P. Hu, D. M. Faulk, J. Wang, K. M. Mayle, K. Bartels, M. Salvatore, A. M. Kinsey, A. N. Demaria, N. Dib and K. L. Christman, *J Am Coll Cardiol*, 2012, **59**, 751-763.
14. J. Xie, X. Zhou, X. Hu and H. Jiang, *Hellenic J Cardiol*, 2014, **55**, 101-106.
15. L. F. S. Bastos, L. A. Merlo, L. T. S. Rocha and M. M. Coelho, *European Journal of Pharmacology*, 2007, **576**, 171-179.

# Chapter 5: Conclusions and future directions

## 5.1 Summary and conclusions

This dissertation aimed to further establish nanomedicine as a platform for drug delivery during the acute phase of myocardial infarction. Specifically, we discussed three polymeric methods for targeted delivery to the infarcted region of the heart: polynorbornene nanoparticles, degradable MePTDO nanoparticles, and polynorbornene protein-like polymers. Utilizing nanoscale platforms for drug delivery is a particularly fitting for applications during the acute phase of MI because they can be administered minimally invasively through intravenous injection. The platforms we have discussed have demonstrated the ability to successfully localize to the infarct and, in some cases, carry a therapeutic molecule.

The first chapter reviewed current nanoparticle platforms that have been engineered to target the injured heart after myocardial infarction. Nanoparticles generally fall into two main categories when discussing their targeting mechanisms: 1) responding or leveraging a facet of the inflammatory response or 2) utilizing a tissue-specific marker to aid in accumulation in the desired organ. Common inflammatory targets include adhesion molecules, pH, ROS, and protease upregulation. The latter playing a large role in the subsequent chapters of this dissertation. Tissue specific markers such as targeting injured cardiomyocytes, mitochondria, and cardiac-specific receptors are also commonly used for localization to the injured myocardium. Overall, the field of targeted nanomedicine demonstrates thoughtful engineering and holds high potential for opening up a crucial window of treatment during the acute phase of MI.

The second chapter expounds upon previously established work utilizing MMP-responsive polynorbornene nanoparticles by assessing its ability to deliver a bioactive therapeutic MMP-inhibitor. As discussed in the first chapter, this platform targets the infarcted region of the heart

through upregulation of MMPs that cleave the polymer backbone, exposing the hydrophobic core and resulting in micron-scale aggregation. Here, we demonstrate that conjugation of a small molecule MMP-inhibitor does not affect the nanoparticle's ability to localize to extravasate out of large vasculature and aggregate in the infarcted heart. *In vitro* evaluation demonstrated that drug incorporation into the nanoparticle increased the concentration at which it could be safely tolerated while also maintaining its ability to inhibit MMP-activity at a comparable level to free drug treatment. Overall, we established this platform as a successful drug carrier that could be modified to bear other therapeutics through chemical modification.

The third chapter explores a degradable nanoparticle platform that maintains the same MMP-responsive mechanism for targeting but is broken down in acidic conditions through the cleavage of phosphoramidate linkages. After verifying that this material maintains its morphological switch after enzymatic cleavage, we then demonstrated that this new nanoparticle was still capable of infarct-specific localization. Comparison of the degradable system with the nanoparticle discussed in Chapter 2 showed distinct differences in biodistribution, specifically in the spleen, kidneys, and left ventricle. We observed a significantly higher degree of degradable nanoparticle accumulation in the infarcted region compared its non-degradable analog. In addition to this, when analyzing heart tissue sections at various timepoints out to 28 days, we observed a significant decrease of degradable nanoparticle presence in the heart as well as all satellite organs. With this, we were able to demonstrate successful degradation and clearance of this material over time.

The fourth chapter establishes a new polymeric material that is not classified as a traditional nanoparticle. The PLP remains as a single polymer chain and does not assemble into spherical micellar structures. Because of this, it acts a low molecular, sub nano-scale entity that

is amorphous, or “protein-like”, in structure. PLPs demonstrated strong colocalization to the infarcted region with morphology that greatly resembled the degradable system, “brush-like” strokes that appeared more like a bolus-style injection into the injured myocardium. In addition to this, PLPs also exhibited highly favorable biodistribution with accumulation primarily in the heart and kidneys, the latter of which is particularly unique and further validates that this material is significantly smaller and has the potential of clearing through urine. Within the infarct, we also observed cellular uptake by injured cardiomyocytes in the necrotic core. This was further validated through an *in vitro* and *in vivo* experiment utilizing propidium iodide to label necrotic nuclei. To better understand the characteristics that contribute to the unique biodistribution and infarct-localization of the PLP, we ran several control studies that demonstrated the importance of amphiphilicity and MMP-responsiveness as methods for improving biodistribution and infarct-targeting.

All in all, these studies have demonstrated the feasibility of three distinct nanoscale polymeric platforms for targeted delivery to the heart during the acute phase of myocardial infarction. While each of these platforms is composed of similar components (polynorbornene, MMP-responsive peptide sequence), we have demonstrated how alterations to the polymer backbone or degree of polymerization can greatly change their behavior *in vivo*. We have shown here that the MMP-responsive nanoparticle is capable of successfully carrying a bioactive small molecule while maintaining the ability to localize to the infarcted region of the heart. The degradable nanoparticle platform demonstrated a significant increase in material accumulation in the heart and clearance from the heart and satellite organs over time due to the incorporation of acid-labile linkages via copolymerization of polynorbornene with MePTDO. Lastly, the PLPs are a representation of a non-spherical platform that primarily localized to the infarcted heart and kidneys due to its smaller size and protein-like morphology which enables significantly longer

circulation times.[1] Additionally, we observed strong interactions between the degradable nanoparticles and PLPs with necrotic cardiomyocytes in the injured heart while the MMP-nanoparticles remain mostly extracellular. All these platforms are an excellent demonstration of how versatile and tunable synthetic materials can be.

Through these studies, we have gained a greater understanding about the importance of certain material characteristics on how our platforms will behave *in vivo*. We hypothesize the size and morphology of the material plays a crucial role in determining the biodistribution and accumulation of these systems *in vivo*. The degradable nanoparticle and PLP systems both represent materials that can either be broken down into smaller fragments or already exist as small, amorphous units, respectively. This allows these systems to have comparable cellular uptake and clearance overtime, something that we do not observe with the MMP-nanoparticle. Additionally, we hypothesize that the amphiphilicity of the materials we work with is crucial to their favorable biodistribution and cellular uptake. Prior to enzymatic cleavage, these systems can traffic through the circulation system as a semi-hydrophilic platform. Once they are cleaved by endogenous MMPs, their hydrophobic core is exposed, leading to aggregation and if the material is small enough, cellular uptake. It has been previously established in a breast cancer cell line that modifying antimicrobial peptides by conjugating long fatty acyl chains to increase their hydrophobicity significantly increased their affinity to cell membranes.[2] We hypothesize that we are observing a similar effect of uptake of hydrophobic aggregates in necrotic cardiomyocytes, but benefit from their amphiphilic nature when the materials are in circulation.

Overall, we hypothesize that these nanoscale platforms demonstrate the ability to bear therapeutic molecules, have favorable and unique biodistribution, and novel cellular interactions.

All three platforms have demonstrated or have the potential for enabling highly efficient drug delivery and therapeutic efficacy in acute myocardial infarction.

### 5.2 Future Directions

The work in this thesis has primarily focused on establishing several nanoparticle platforms as successful platforms for delivery during the acute phase of MI. Now that we have a concrete understanding of the various localization, retention, and clearance patterns of each platform: the polynorbornene nanoparticle, degradable nanoparticle, and protein-like polymer, we can begin to think about what sort of therapeutic would be most relevant for delivery. Particularly for the degradable nanoparticle and PLP platforms, it is important to consider the kinds of cells these platforms primarily appear to interact with, namely, necrotic cardiomyocytes and $CD68^+$ macrophages. With this knowledge, we could consider administering cardioprotective molecules or therapeutics for polarization of macrophage populations. Additionally, it is important to consider the timeline of material retention in the heart, which varies depending on the platform, from ~1 month (degradable nanoparticles) to indefinitely (polynorbornene nanoparticles).

While we have demonstrated successful targeting through the incorporation of an MMP-responsive polymer backbone, we are also interested in exploring new targets that may allow for higher tissue-specific delivery. A previous that used *in vivo* phage display discovered a cardiac homing peptide sequence that demonstrated strong affinity for binding to the injured myocardium.[4] Incorporation of these new substrates into our various polymer platforms could allow for enhanced delivery to the heart.

As was discussed in chapter 3 and 4, molecular weight or the generation of smaller molecular weight fragments as well as the water solubility of a material have a profound effect on biodistribution and cellular interactions. With this in mind, we could consider designing materials

of varying molecular weights and solubilities to assess how this shifts patterns in biodistribution, circulation time, and retention. This kind of work would further optimize the polymer systems we work with as well as characterize the diverse behavior of our platforms for other potential disease pathologies.

Additionally, we hypothesize that the platforms we have developed in this work are not only applicable in acute myocardial infarction. They could be applied to many other inflammatory conditions in which MMPs are upregulated. Our lab has also done work with a model of necrotic skeletal muscle and acute traumatic brain injury, and we are interested to see how these polymeric materials might behave in a new disease pathology.

### 5.3 References


1. C. E. Callmann, M. P. Thompson and N. C. Gianneschi, *Accounts of Chemical Research*, 2020, **53**, 400-413.
2. Y. Yang, H. Zhang, Y. Wanyan, K. Liu, T. Lv, M. Li and Y. Chen, *ACS Omega*, 2020, **5**, 21513-21523.
3. A. Cuadrado, A. I. Rojo, G. Wells, J. D. Hayes, S. P. Cousin, W. L. Rumsey, O. C. Attucks, S. Franklin, A.-L. Levonen, T. W. Kensler and A. T. Dinkova-Kostova, *Nature Reviews Drug Discovery*, 2019, **18**, 295-317.
4. S. Kanki, D. E. Jaalouk, S. Lee, A. Y. Yu, J. Gannon and R. T. Lee, *J Mol Cell Cardiol*, 2011, **50**, 841-848.